Reliability and Degradation Characterization for PV Modules and Systems

by

Alexander C. Killam

A Dissertation Presented in Partial Fulfillment
of the Requirements for the Degree
Doctor of Philosophy

Approved April 2022 by the
Graduate Supervisory Committee:

Stuart Bowden, Chair
Michael Goryll
André Augusto
James Rand

ARIZONA STATE UNIVERSITY

May 2022

ABSTRACT

In-field characterization of photovoltaics is crucial to understanding performance and degradation mechanisms, subsequently improving overall reliability and lifespans. Current outdoor characterization is often limited by logistical difficulties, variable weather, and requirements to measure during peak production hours. It becomes a challenge to find a characterization technique that is affordable with a low impact on system performance while still providing useful device parameters. For added complexity, this characterization technique must have the ability to scale for implementation in large powerplant applications.

This dissertation addresses some of the challenges of outdoor characterization by expanding the knowledge of a well-known indoor technique referred to as Suns-V_{OC}. Suns-V_{OC} provides a pseudo current-voltage curve that is free of any effects from series resistance. Device parameters can be extracted from this pseudo I-V curve, allowing for subsequent degradation analysis. This work introduces how to use Suns-V_{OC} outdoors while normalizing results based on the different effects of environmental conditions. This technique is validated on single-cells, modules, and small arrays with accuracies capable of measuring yearly degradation. An adaptation to Suns-V_{OC}, referred to as Suns-Voltage-Resistor (Suns-VR), is also introduced to complement the results from Suns-V_{OC}. This work can potentially be used to provide a diagnostic tool for outdoor characterization in various applications, including residential, commercial, and industrial PV systems.

DEDICATION

Dedicated to my beloved parents, Jillian and Matthew Killam. You will always be my biggest heroes.

ACKNOWLEDGMENTS

Throughout the tenure of my PhD, I have received an incredible amount of support and guidance. One page is not enough to mention every person who has helped provide a positive impact to both this work and my life.

I would first like to thank my professor, Stuart Bowden. You helped shape my way of thinking and guided me towards a more scientific process. I can't thank you enough for allowing me to become a part of the silicon research group at SPL. I would like to thank Michael Goryll for always being supportive within every research/outreach venture, no matter how irrelevant to your own research. Thank you to Jim Rand for providing a new perspective on my research and providing me with the knowledge you have gained from the industry. Lastly, I would like to thank André Augusto for providing the mentorship that helped me persevere to the end. I would have likely stopped years ago if it wasn't for you.

I would like to thank all my past colleagues within QESST including the staff, faculty, and students. There are way too many names to mention all, but I particularly would like to mention Alex Routhier and Srinath Murali. You two have provided the best support that any friend could ever wish for. Thank you to my parents Matt and Jill and my brothers Tristan and Liam for your understanding and your encouragement when I made the decision to move across the country to pursue this venture. And finally, I would like to thank my partner Kristen Cook for everything. You have supported me in so many ways and through so much, this wouldn't have been possible without you.

TABLE OF CONTENTS

Page

CHAPTER Page

LIST OF TABLES

Table Page

LIST OF FIGURES

Figure Page

Figure Page

Figure Page

1 INTRODUCTION

By 2020, over 760 GW of photovoltaic (PV) systems were installed throughout the world, representing 3.7% of the world electricity demand, and over 2 billion PV modules operating in multiple climates under varying weather conditions [1]. More than two-thirds of those modules were installed in the last 5 years, often using new designs and new solar cell technologies [2]. Not enough time has passed to subject those new module designs to long-term field reliability studies. Understanding the degradation rate and risk of failure of PV systems is critical to predict the levelized cost of electricity (LCOE), an extremely important metric for system owners, financiers, and other stakeholders in the PV industry [3], [4].

Indoor standard accelerated stress testing, namely the IEC 61215 standard for terrestrial PV modules [5], is a valuable methodology to identify fault mechanisms, estimate the degradation rate, and to ensure the safety and normal operation of modules in the field. Standardized tests help module and cell manufacturers to identify and mitigate faults early in the development phase, reducing the time-to-market of new products [6]. However, these tests fail to predict some of the faulting mechanisms observed in the field [7]. In recent years, the National Renewable Energy Laboratory (NREL) developed combined-accelerate stress testing to surpass some of the limitations of the conventional single factor stress tests [8]. The multi-factor testing is an important achievement in indoor accelerated testing, where modules are subjected to conditions closer to those experienced in the field. Yet, these tests are still an incomplete image of the exact stress mechanisms

that PV systems are subject to outdoors, which vary with location, time of day, and time of year [9].

Presently, various outdoor characterization techniques have proven effective in identifying degradation mechanisms and faults. Some of these characterization techniques are discussed in Chapter 2. This chapter also discusses how these outdoor techniques account for variable environmental conditions and translate results to a standardized set of conditions. This work capitalizes on a characterization technique called Suns-Open Circuit Voltage (Suns-V_{OC}), which is widely used for laboratory measurements of single solar cells. The underlying theory of indoor Suns-V_{OC} is introduced in Chapter 3. This chapter also discusses how the Suns-V_{OC} technique can be adapted for outdoor applications. Simulation Program with Integrated Circuit Emphasis (SPICE) modeling was conducted to support the theories for outdoor implementation. The experimental results of outdoor implementation are then presented. The characterization technique was first tested on a single-cell PV module, where it could be tested indoors to verify outdoor results. Subsequent testing was then performed on a 96-cell module, representing a typical commercially available PV module. Temperature corrections were performed using both backsheet temperature sensors and a local weather station, providing feasibility for scalable applications. Finally, testing was then performed on a 4-module array, an analog to a conventional PV string.

A novel characterization technique, referred to as Suns-Voltage-Resistor (Suns-VR) is then introduced in Chapter 4 as a complement to Suns-V_{OC}. Simulations and indoor

experimental testing were conducted as proof of concept. This work can ultimately be expanded on to test the validity of outdoor usage.

The impact and potential applications of outdoor characterization are presented in Chapter 0. The PV industry can be further accelerated by adequate testing and measurements of PV systems and modules. This dissertation seeks to demonstrate that the PV industry must continue to rely on various forms of outdoor characterization to meet the reliability and cost goals of both the present and future. Final opportunities and conclusions are presented in Chapter 6.

2 BACKGROUND

The energy from the sun is the most abundant source of free energy, providing more energy to the earth in a day than the global population uses in an entire year [10]. Photovoltaics are typically semiconducting materials that convert light into electricity by utilizing the photovoltaic effect [11]. Photovoltaic systems may suffer from various degradation mechanisms, influenced by cell/module architecture, installation, racking, weather, and climate. Characterization is key to understanding these degradation mechanisms and their causes. This chapter includes the theoretical background of PV module and system operation. A thorough analysis is then presented, examining the impacts of outdoor conditions on a PV module's I-V characteristics. The chapter concludes with a detailed review of different outdoor characterization techniques currently used to monitor PV systems and identify degradation mechanisms.

2.1.1 Current-Voltage Characteristics

Current-Voltage (I-V) measurements are the photovoltaic industry standard for characterizing and ranking the performance of solar cells and modules. For example, the datasheet of a module is given in terms of the I-V characteristics and power output under different conditions. The I-V curve is a changing snapshot of the operation of a cell or module and can be used to gauge the degradation based on deviations of their characteristics over time. Figure 2.1 gives an example of I-V and power-voltage (P-V) curves for a generic 72-cell PV module. The I_{SC} and I_{MP} are the short-circuit and maximum-power currents, and the V_{OC} and V_{MP} are the open-circuit and maximum-power voltages. The M_{PP} is the maximum-power point and is the product of V_{MP} and I_{MP}.

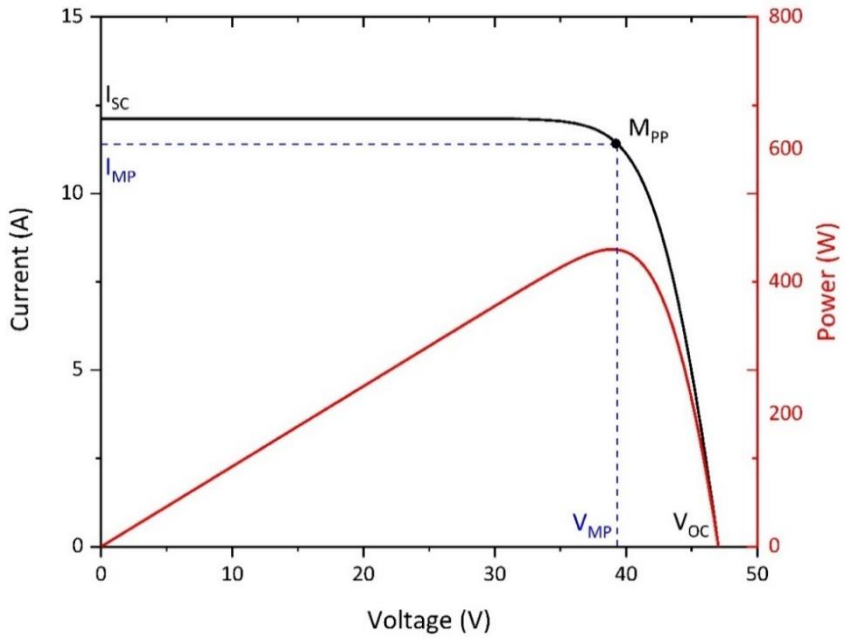

Figure 2.1. Simulated I-V and P-V Curve of a 72-Cell PV Module [12].

The fill factor (FF) represents the "squareness" of the I-V curve and can be determined by the following equation:

$$FF = \frac{V_{MP} \times I_{MP}}{V_{OC} \times I_{SC}} \tag{1}$$

The FF can also be graphically determined by taking the ratio of area between the two squares shown in Figure 2.2. The FF is commonly used to gauge performance because it embodies many of the loss mechanisms that impact the solar cell. As the FF is a ratio, it is less dependent upon the environmental conditions than I_{SC} or V_{OC}. The efficiency (η) of the module is the ratio of output power to input power, as shown in the following equation:

$$\eta = \frac{P_{out}}{P_{in}} = \frac{FF \times V_{OC} \times I_{SC}}{E \times Area} \tag{2}$$

The E represents the incident irradiance as Watts/m^2 on the collecting area of the module. Module efficiencies are lower than cell efficiencies for several reasons. The

module area is slightly larger than the sum of the areas of the individual cells as the module area also includes the space between the cells and the frame. The encapsulant and front sheet used for the module can absorb and reflect photons, which results in a lower overall external quantum efficiency. The material typically used as a backsheet can reflect more photons back to the cells, easing some of the losses due to the front sheet and encapsulant.

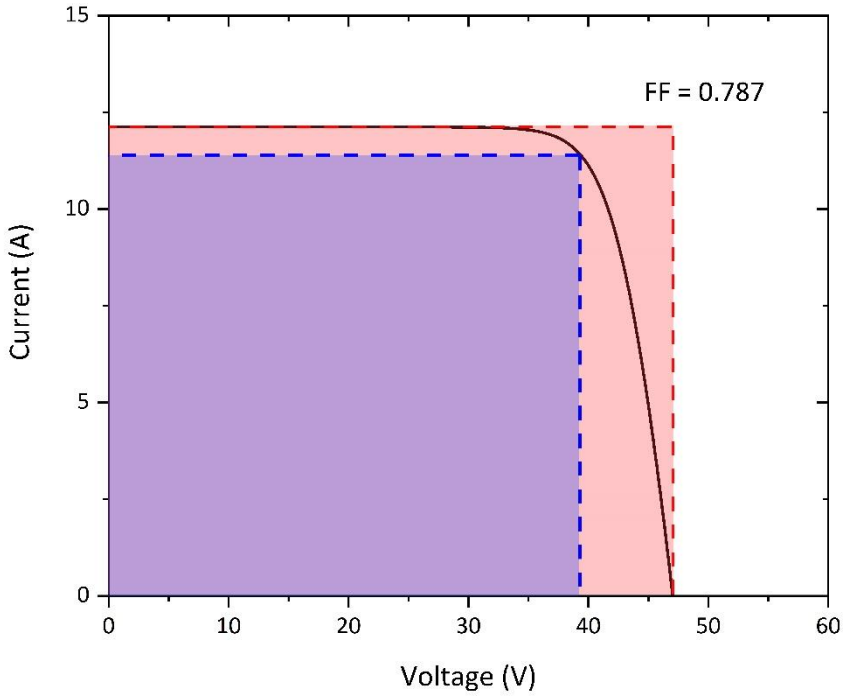

Figure 2.2. Graphical Representation of Fill Factor for a 72-Cell PV Module.

2.1.2 Single Diode Equivalent Circuit for a PV Cell

To better understand the electrical output of a PV cell, an electronically equivalent model is presented in Figure 2.3. This model is referred to as the single diode model and describes the dominant performance and loss metrics with.

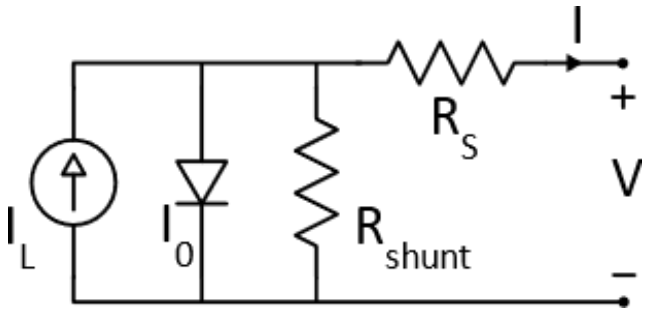

Figure 2.3. Single Diode Equivalent Circuit for a PV Cell.

The circuit elements describe the I-V characteristics of the cell and are mathematically represented by the following equation:

$$V = I_L - I_0\left[e^{\frac{V+IR_S}{nV_T}} - 1\right] - \frac{V + IR_S}{R_{shunt}} \quad (3)$$

The parameters of (3) are described in the context of commercial silicon solar cell modules [13]. The light generated current (I_L) is a function of the light incident on the solar cell, and its behavior in practice is close to ideal. There is a linear relationship between I_L and light intensity over several orders of magnitude. In addition, the assumption of I_L as being constant with applied voltage is also generally valid. The variation of I_L with temperature follows the response that would be expected from changes in light absorption caused by the bandgap shift with temperature. Furthermore, I_{SC} is equivalent to I_L unless the module is particularly degraded with a very high series resistance (R_s) and a low shunt resistance (R_{shunt}).

The dark saturation current (I_0) describes the recombination in the device and the operation of the diode [14]. An ideal diode has a constant recombination lifetime so that there is a single I_0 over the entire voltage range. In practice, the recombination mechanisms change with minority carrier concentration and so operating voltage. To capture the

variation in I_0, the ideality factor (n) is introduced. It is typically close to one and describes the changes in recombination over typical device operation from V_{MP} to V_{OC}. The I_0 also increases dramatically with temperature leading to a loss in V_{OC}. The following equation defines the thermal voltage, V_T:

$$V_T = \frac{kT}{q}, \tag{4}$$

where k is Boltzmann's constant, q is the electronic charge, and T is the temperature.

The R_{shunt} can often be neglected in monocrystalline silicon modules. For multicrystalline silicon modules, the behavior of R_{shunt} is more complicated [15]. It is more accurately described as a shunting mechanism that can be characterized as a diode or diodes separated by a resistance [16]. The R_S is presented as a single value that captures all the individual resistances within the cell such as finger resistance. However, the resistive losses are distributed throughout the cell in a network that includes the diode elements. The flow of current within the cell changes depending on the operating point (e.g. with illumination or voltage) and thus the apparent resistance also changes [17].

Given the changing nature of the parameters, I_0, R_S and R_{shunt}, one may wonder about the usefulness of equation 1. However, these parameters are nearly constant over a practical range of module operation and determined from experimental data. For example, a typical module datasheet provides I-V curves over the range of 200 to 1000 W/m^2 and a temperature of 5°C to 65°C [18]. The derived model is semi-empirical, and it has validity and predictive power over the measurement range.

The single-diode model is widely used to model the output characteristics of a PV cell because it simplifies the output by assuming a constant value for the ideality factor,

though this assumption is sometimes invalid and can lead to inaccuracies. For example, at high operating voltages, recombination is dominated by the surfaces and bulk regions, resulting in an ideality factor close to one. At low operating voltages, recombination dominates within the junction resulting in an ideality factor much closer to two. Because of this phenomenon, a second diode is used and referred to as the double diode model. As the name implies, the double diode model uses a second parallel diode, which typically has an ideality factor of two to account for junction recombination. For silicon devices, the double diode model often provides invalid results because of the intricacy of recombination and the relationship with carrier concentration. Therefore, this work is built on the single-diode model, with varying ideality factors as a function of voltage.

2.2 Photovoltaic Characterization Outdoors

Indoor standard accelerated stress testing, namely the IEC 61215 standard for terrestrial PV modules [5], is a valuable methodology to identify fault mechanisms, estimate the degradation rate, and to ensure the safety and normal operation of modules in the field. Standardized tests help module and cell manufacturers identify and mitigate faults early in the development phase, reducing the time-to-market of new products [6]. However, these tests fail to predict some of the faulting mechanisms observed in the field [7]. In recent years, the National Renewable Energy Laboratory (NREL) developed combined-accelerate stress testing to surpass some of the limitations of the conventional single factor stress tests [8]. The multi-factor testing is an important achievement in the indoor accelerated testing, where modules are subject to conditions closer to the ones experienced in the field. Yet, these tests are still an incomplete image of the exact stress mechanisms

that PV systems are subject to outdoors, which vary with location, time of day, and time of year [9].

Outdoor diagnostic methods are then required to assess the performance and reliability of the PV systems in the relevant environments. Identifying the reasons why individual elements of the PV systems are underperforming is particularly significant for new module designs with only a few years of field installation [3]. Outdoor diagnostics are extremely valuable for the solar industry, providing important guidance for future cell, module, and system designs, particularly in the context of an industry which is positioning to offer 50-year module warranties [19]. Presently, several outdoor imaging-based characterization techniques have proven to be effective in identifying module faults [20]–[23]. Many of these techniques have the advantage of acquiring data over large areas in a reasonable short period. There is no question about the importance of these techniques, especially among PV plant owners, but they are limited to the extent of not providing quantitative information regarding the nature of each faulting mechanism [3]. To investigate the different degradation modes and their root causes, current–voltage (I–V) measurements of modules are highly desirable [24]. Using outdoor environments, we can measure the I-V characteristics of modules under real operation conditions and extrapolate parameters such ideality factor and injection-dependent lifetime, gaining more detailed understanding of the underlying degradation mechanisms [25], [26].

The following section reviews some of the more popular methods currently used to characterize PV systems operating in the field. The impacts of outdoor conditions are

discussed, including techniques and standards used to translate outdoor results to standard testing conditions.

2.2.1 Outdoor Effects on I-V Characteristics

Modules are typically measured indoors under Standard Test Conditions (STC, per IEC TS 61836) before being installed in the field [27]. Indoor STC measurements are controlled for a specific irradiance (1000 W/m^2), temperature (25 °C), and a standard spectrum of AM 1.5G [28]. The STC is not intended to duplicate the exact range of conditions that modules experience in the field, but to provide a reasonable baseline for meaningful comparison in the industry. Though there are issues with replicating the sun spectrum, these indoor measurements are simpler, as they are not impacted by the transient outdoor effects. In the field, the outdoor conditions dramatically influence the electrical properties of the modules. As a result, it is critical to measure those conditions and to understand how they affect the performance of the modules, otherwise it is not possible to evaluate if potential deviations in the module performance are due to fluctuations of the environmental conditions or due to the module itself [29].

The AM (air mass) 1.5G is the only reference spectrum used for indoor STC measurements of modules, even though the solar spectrum outdoors undergoes constant changes due to angle of incidence, aerosols, water vapor, among others [30]–[33]. The AM 1.5G captures both the direct and normal irradiance (hence the G for global) that reaches the surface when the sun passes through 1.5 atmospheres. The irradiance that modules experience outdoors is rarely equivalent to the AM 1.5G spectrum used for indoor STC

measurements but has been recognized as the standard embodying the average across all outdoor regimes. Spectral deviations from the AM 1.5G standard result in direct changes in current production, with more severe impacts on amorphous silicon (a-Si) modules [34]–[36]. The spectral impact on module performance must be understood because of the changes based on season, time of day, and geographic location.

The output current of a module has a proportionate relationship to the amount of incident light, as shown in Figure 2.4. Consequently, partial shading may result in major disruptions to performance and outdoor measurements. Partial shading may be a result of cloud coverage, telephone poles, interrow shading, bird droppings, soiling, and others. Soiling is an accumulation of dust, snow, or other particles that may be shadowing the front surface of a solar module [37], [38]. Soiling is more critical in desert regions, especially northern Africa and the Middle East, due to low precipitation and high dust deposition [39]. The impact of soiling can be measured via I-V measurements but can be mitigated after cleaning [40]. The result of shading manifests in the module output by a dramatic decrease in current, due to the conventional series configuration of solar modules [41]. Once a cell is shaded, the bypass diode for that respective string is activated, showing a major reduction in the current portion (or "step") of the I-V curve [42]. A comprehensive review of partial shading impacts on PV can be found here [43].

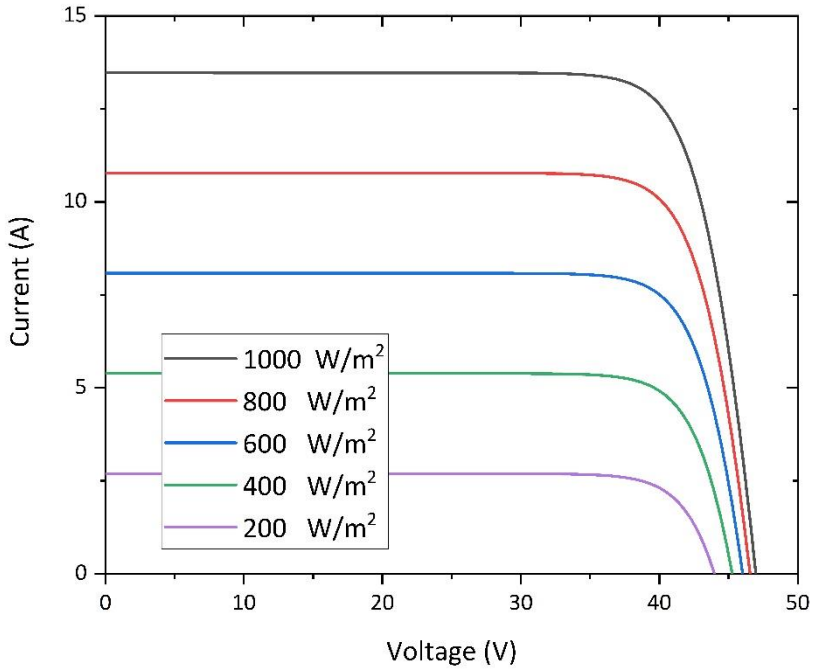

Figure 2.4. Simulated I-V Curve of 72-Cell Module with Variable Irradiance [12].

As the operating temperature increases, the semiconductor bandgap decreases, resulting in a reduction of V_{OC} due to an increase in I_0 [29]. The decrease in bandgap energy also causes a slight increase in I_{SC}, as more incident photons have sufficient energy to generate electron-hole pairs [44]. The reduction of voltage is much greater than the increase of current, resulting in an overall decrease of power with increased temperatures [45]. Figure 2.5 displays the resulting I-V curves of a typical 72-cell module for different operating temperatures. The temperature dependence depends on the cell architecture, module configuration, wind speed, mounting configuration, etc. [46]–[48]. This dependence must be understood to ensure proper temperature translations during outdoor characterization.

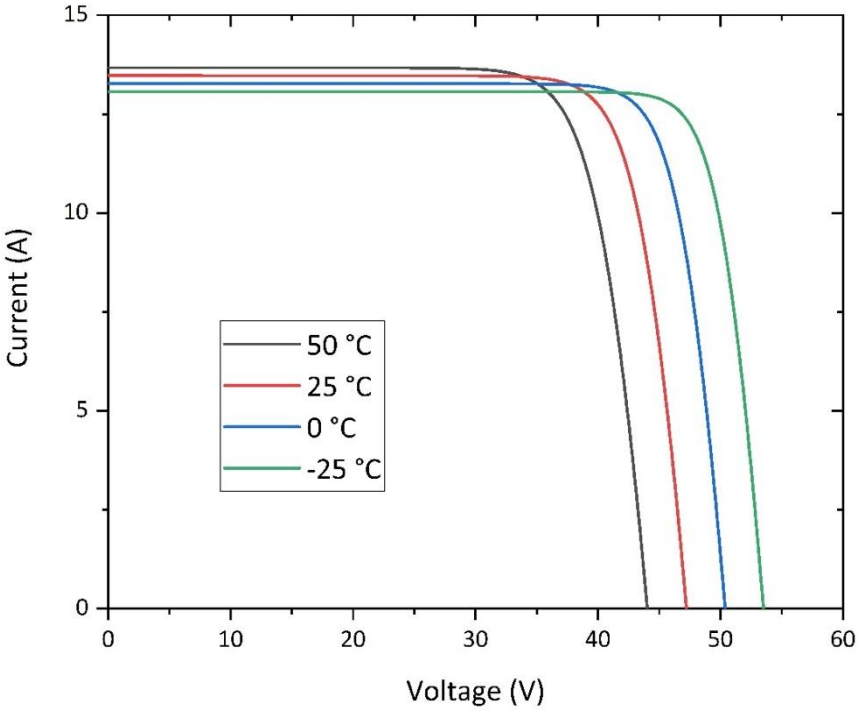

Figure 2.5. Simulated I-V Curve of 72-Cell Module with Variable Operating Temperature [12].

All the mentioned outdoor effects can significantly affect the resulting I-V curves. Without proper identification, environmental influences can be misinterpreted as module degradation. For example, the IEC 62446-1 categorizes six types of deviations that are numbered in Figure 2.6 [49]: (1) bypass diode(s) activation caused by cell mismatch or partial shading, commonly referred to as “steps”; (2) low current output caused by uniform shading or degradation; (3) low voltage output caused by increased temperature, bypass diode failures, or degradation; (4) rounded knee near maximum power point caused by degradation; (5) increased series resistance caused by wiring issues or degradation; and (6) increased shunt resistance caused by mismatch or degradation. These deviations are a consequence either from environmental conditions or module degradation, or both.

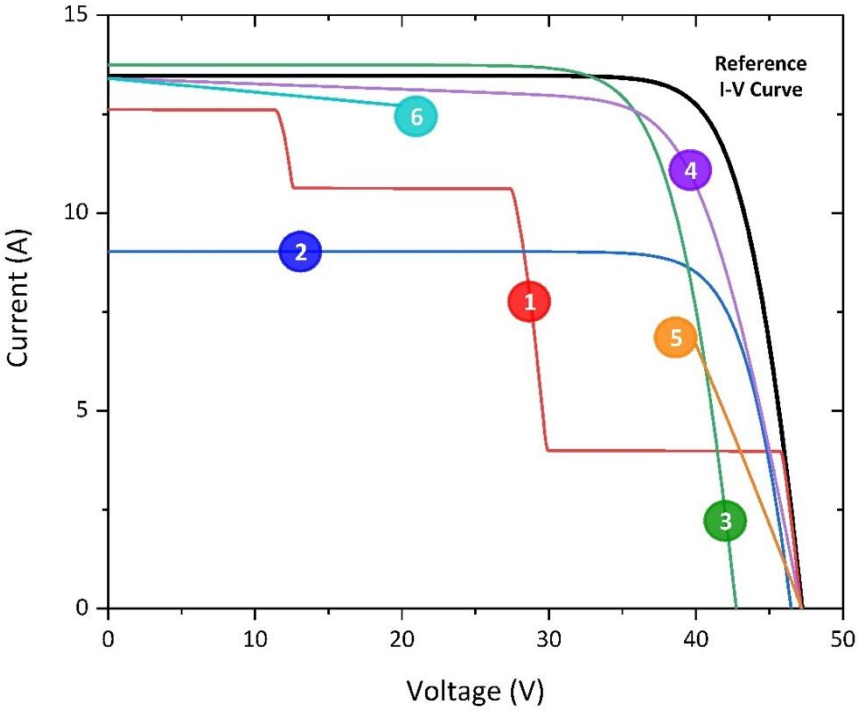

Figure 2.6. Result of I-V Curve Deviations Where Numbers One to Six Are Described in IEC 62446-1 [12].

2.2.2 STC Translations of I-V Characteristics

Outdoor I-V measurements can be used to monitor the PV performance via model-based difference analysis and correction-based analysis [50]. Model-based difference analysis relies on comparing measured and simulated I-V characteristics for a certain outdoor condition. Correction-based analysis relies on correcting the entire I-V measurement to a particular set of conditions, typically STC. The PV community is constantly developing and improving models and techniques for this translation, but most rely on the techniques outlined in IEC 60891 [51]. The standards provide multiple empirical and semi-empirical methods of translating I-V curves to different temperatures

and irradiances, including those widely used in the industry but not codified into international standards [52]. These standards are explained in the following paragraphs.

The first technique is empirically driven and based on the work from the Jet Propulsion Laboratory [53]. To use this technique, one must know the temperature coefficients for current (α), voltage (β), and series resistance (κ). The first technique uses the following two equations:

$$I_2 = I_1 + I_{SC}\left(\frac{G_2}{G_1} - 1\right) + \alpha(T_2 - T_1) \quad (5)$$

$$V_2 = V_1 - R_S(I_2 - I_1) - \kappa * I_2(T_2 - T_1) + \beta(T_2 - T_1) \quad (6)$$

Where, I_1 and V_1 are the measured current-voltage points from the I-V curve, I_2 and V_2 are the resulting translated current-voltage points, G_1 and T_1 are the measured irradiance and temperature, G_2 and T_2 are the standard or preferred irradiance and temperature to be translated to, α and β are the temperature coefficients for current and voltage, R_S is the internal series resistance of the device under test, and κ is the curve correction factor.

The second technique is semi-empirical, based on the single-diode model. This methodology requires five different coefficients. The first termed α is the irradiance correction factor for the open-circuit voltage, which is related to the diode thermal voltage. As a replacement to α and β, an initial coefficient κ′ is used to account for temperature induced changes to the fill factor and the internal series resistance. Temperature coefficients for current and voltage are expressed as α_{rel} and β_{rel}, which are normalized coefficients of the test module measured at STC irradiance. This technique better defines

the I-V points near the maximum power point, providing more accuracy for maximum power approximation. This technique relies on the following two equations:

$$I_2 = I_1\left(1 + \alpha_{rel}(T_2 - T_1)\right)\frac{G_2}{G_1} \tag{7}$$

$$V_2 = V_1 + V_{OC1}\left(\beta_{rel}(T_2 - T_1) + a\ln\frac{G_2}{G_1}\right) - R'_S(I_2 - I_1) - \kappa' * I_2(T_2 - T_1) \tag{8}$$

Where, I_1 and V_1 are the measured current-voltage points from the I-V curve, I_2 and V_2 are the resulting translated current-voltage points, G_1 and T_1 are the measured irradiance and temperature, G_2 and T_2 are the standard or preferred irradiance and temperature to be translated to, V_{OC1} is the measured open-circuit voltage at G_1 and T_1, α_{rel} and β_{rel} are the normalized temperature coefficients for current and voltage, a is the irradiance correction factor, R'_S is the internal series resistance of the device under test, and κ' is the curve correction factor.

The third technique relies on a linear interpolation methodology. This method relies on two assumptions as follows: The I-V curve is the sum of both the dark current and photocurrent, which is proportional to the irradiance or I_{SC}. The output voltage has a linear relationship with temperature when the output current is constant [54]. This technique is free from needing any correction coefficients but does need an interpolation constant. At least two separate I-V curves are needed to perform the linear interpolation for a specified irradiance or temperature. Three curves would be needed to translate to both irradiance and temperature. The interpolation is completed by solving for the interpolation constant via the following four equations:

$$I_3 = I_1 + \gamma(I_2 - I_1) \tag{9}$$

$$V_3 = V_1 + \gamma(V_2 - V_1) \quad (10)$$

$$G_3 = G_1 + \gamma(G_2 - G_1) \quad (11)$$

$$T_3 = T_1 + \gamma(T_2 - T_1) \quad (12)$$

Where, I_1 and V_1 are the measured current-voltage points from the first I-V curve at irradiance level G_1 and temperature level T_1, I_2 and V_2 are the measured current-voltage points from the second I-V curve at irradiance level G_2 and temperature level T_2, and I_3 and V_3 are the measured current-voltage points from the third I-V curve at irradiance level G_3 and temperature level T_3, and γ is the interpolation constant.

2.2.3 Environmental Sensors

The quality of the STC translations is determined by the quality of the measured environmental conditions. The two most relevant parameters are operating temperature and incident irradiance. Since these parameters are difficult to measure, models to translate ambient measurements to cell operating conditions are used. The resulting uncertainty of these models is the dominant contribution to the overall uncertainty of predicted performance [55]. One technique to reduce the uncertainty is known as "sun-shading," where the module is cooled down to be measured closer to the STC temperature [56].

The most common method for measuring irradiance is with a thermopile pyranometer. Thermopile pyranometers are thermocouple-based devices with two surfaces, one heated with incident irradiation and one that does not absorb solar radiation. The resulting difference between the two temperatures is indirectly related to irradiance [57]. They measure irradiance within the spectral range of 300-2800 nm [58]. Silicon

photodiode pyranometers are a low-cost alternative to thermopile pyranometers [59]. These photodiode pyranometers capitalize on the photovoltaic effect by converting incident irradiance to an output current, within the spectral range of 400-1100 nm [58]. As an analog to photodiode pyranometers, reference solar cells have been used to measure irradiance. The use of reference cells can be beneficial by having a similar angular response, architecture, and material properties of the measured module [60]. Numerous studies have been conducted to analyze the different sensor technologies, with differing results [61]–[69].

As previously discussed, the temperature of the cells within a module has a strong impact on the module voltage (power) output. Since the modules are encapsulated, it is not possible to directly measure the temperature of the cells. A common practice is to measure the module's average backsheet temperature. The backsheet temperature measurement is outlined in the standard IEC 60891 and requires at least four temperature sensors [51]. The most used temperature sensors are resistance temperature detectors (RTD), thermocouples, integrated circuit (IC) semiconductor-based, and non-contact infrared (IR). The thermocouple and IC sensors have been frequently used due to their low cost but are typically packaged in shapes that make for poor thermal insulation and physical contact with the modules, resulting in lower accuracy. The RTD and IR sensors result in much higher accuracy but cost more than the previously mentioned alternatives. More details on the characteristics of these sensors can be found in [70]–[74].

2.2.4 Outdoor Characterization Techniques

Characterization has been a major tool for the PV industry. The last standardized form of characterization typically takes place upon the completion of a PV module via a flash testing I-V trace. For many years, that was the last form of testing that took place for PV modules. Though recently, characterization has become a tool to also use in the outdoor setting. This section outlines some of the most common outdoor characterization techniques.

2.2.4.1 I-V Curve Tracing

Current-Voltage (I-V) tracing is by far one of the most common and useful characterization techniques. Several recent reviews describe I-V curve tracing methods [75]–[78]. The basic principle of I−V curve tracers is to measure the variation of current and voltage from the open-circuit to short-circuit condition by applying a variable load. There are five methods to perform this task: (1) variable resistor; (2) capacity load; (3) electronic load, which includes the bipolar power supply; (4) four-quadrant power supply; and (5) DC–DC converter. Table 2.1 summarizes the tradeoffs associated with each I-V method in terms of: (1) accuracy – the degree to which the measurement conforms to the correct values; (2) resolution – the frequency of measurement points for the I-V curve; (3) sweep speed – the overall speed of the I-V sweep; (4) fidelity – the ability to measure all points of the I-V curve, specifically I_{SC} and V_{OC}; (5) modularity – the ability to reduce/combine tracers for smaller/larger applications; (6) cost – the cost associated with the technique based on relative comparison to one another; and (7) maximum power rating – the maximum power the tracer can accept from the PV output.

Table 2.1. Tradeoffs Associated with Different I-V Curve Tracing Methods Where 1 Is [75], 2 Is [77], and 3 Is [76] as Found in [12].

Method	Accuracy 2,3	Resolution 2,3	Sweep speed 1,2,3	Fidelity 1,3	Modularity 1,3	Flexibility 1,3	Cost 1,3	Maximum Power Rating 2,3
Resistive load	Low	Low	Low	Medium	Medium	Medium	Low	Low
Capacitive load	Medium	Medium	Medium	Medium	Low	Low	High	High
Electronic load	Medium	Medium	Medium	Medium	High	High	High	Low
Four quadrant power supply	High	High	High	High	Low	Low	High	Low
DC-DC converter	High	High	Medium/High	High	High	High	Low	High

I-V tracing provides a detailed snapshot of the PV module's electrical performance. I-V tracing is the final quality check for a PV module before being delivered to the install location. When PV modules are believed to be underperforming, an I-V trace is needed to qualify for warranty claims. As valuable as I-V tracing is, it can be cumbersome for large PV installations due to logistical hurdles. This obstacle can be overcome by using in-line I-V tracers that are permanent hardware but are also more costly.

2.2.4.2 Visual Inspection

The process of investigating visual artifacts found in fielded modules is referred to as visual inspection. Visual inspection may seem inessential, but that couldn't be more wrong. It is one of the quickest and cheapest techniques that can be used to evaluate many defects. Table 2.2 provides a list of silicon PV module/system failures that can be diagnosed via visual inspection according to IEC 61215 [5], as outlined in the IEA Report [79].

Table 2.2. PV System Failures Diagnosable by Visual Inspection According to IEC 61215.

Component	**Failure Descriptions**
Frontsheet	Bubbling, delamination, yellowing, browning
PV Cell	Cracks, discolored antireflection
Metallization	Burns, snail trails
Frame	Structural damage, scratches
Backsheet	Bubbling, delamination, yellowing, burns
Junction Box	Oxidized, corroded
Connectors	Brittle, broken, exposed wiring, cut wiring, corroded

Visual inspection can be one of the most valuable characterization tools available, but only if conducted properly. NREL developed reporting documentation, consisting of 14 different sections, to collect data for visual inspection [80]. The downside to this technique is that is takes approximately 4-5 minutes for two experienced technicians to inspect a single module. Also, some degradation may only be seen in the electrical parameters, invisible to visual inspection. Though, the low cost and effort of visual inspection has proved valuable. It was successfully used to detect yellowing encapsulation, as shown in Figure 2.7, which is a sign of degradation due to the formation of acetic acid [81].

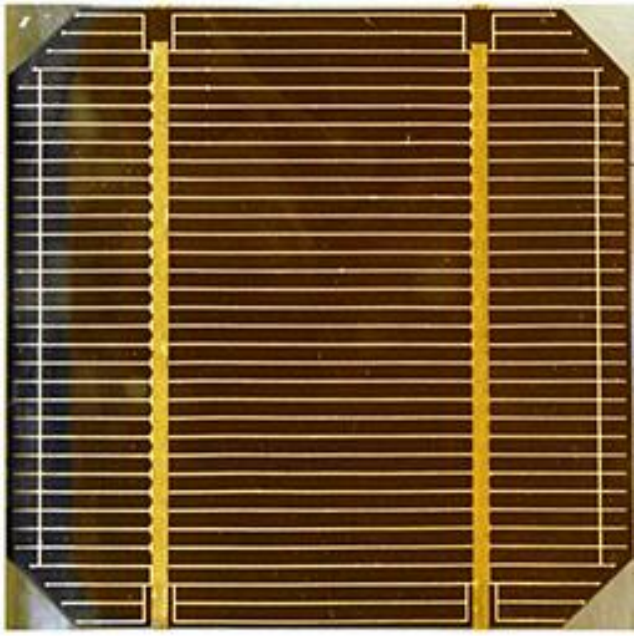

Figure 2.7. A PV Cell Suffering from Yellowing Encapsulation Identified Through the Use of Visual Inspection By [81].

2.2.4.3 Performance Ratio

Photovoltaic systems are comprised of much more than just PV modules. In the case of a poor-performing system, it cannot be assumed that the poor performance is solely due to the PV modules. In this case, performance ratios are used to define the performance of the entire system. The performance ratio is defined in IEC 61853-1 as the ratio of final energy yield to the reference energy yield [82]. The final energy yield is defined as the ratio of net output energy to the DC nameplate rating. The reference energy yield is the ratio of actual irradiance to the STC reference irradiance.

Performance ratios are typically used by PV plant operators and can provide a "health check" of the system. Performance ratios have been calculated with frequencies

ranging from daily to annually. A study conducted in Turkey showed that performance ratios can vary by +/- 12% from month to month [83].

2.2.4.4 Thermography

Thermography is likely the most common characterization technique performed at the utility scale. There are three different types of thermography being steady-state, pulsed, and lock-in thermography. Steady-state imaging can be conducted during normal PV operation as a non-contact solution. Pulsed and lock-in thermography provide a more quantitative picture but are difficult to do in outdoor conditions.

Steady-state thermography is conducted by measuring the direct and indirect heat in the PV module via an infrared (IR) camera. The heat is generated from the incident light which allows for imaging to be conducted during sun hours. When a cell or module is suffering from an issue, the heat is exacerbated and can easily be seen in the IR image. This technique can diagnose several issues including but not limited to broken wiring, partial shading, bypass diode failure, shunting, etc. Drones have been used to perform quick IR imaging for power loss predictions, resulting in accuracies comparable to power measurements [84]. An example of a broken cell captured via IR imaging is displayed in Figure 2.8 [85]. Thermography is an excellent solution for high throughput and affordable characterization for the outdoor utility setting.

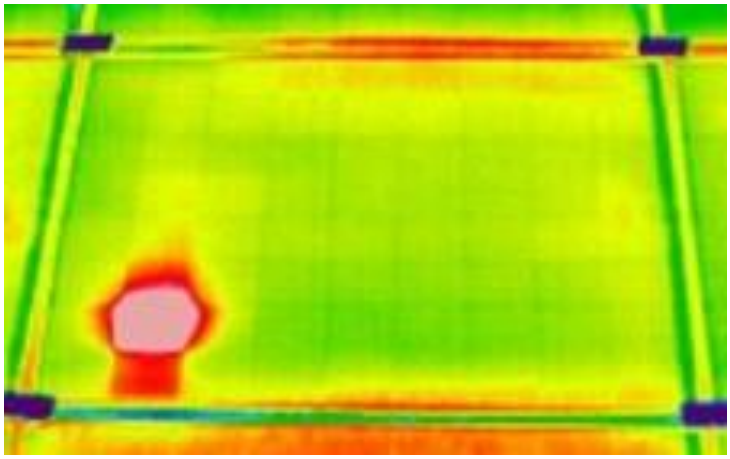

Figure 2.8. A Broken PV Cell Identified Through the IR Thermography By [85].

3 SUNS-V_{OC}

The characterization technique Suns-V_{OC}, also termed illumination-V_{OC}, is the process of measuring the device's open-circuit voltage with varying light intensity. From the Suns-V_{OC} measurement a pseudo I-V curve is generated, which is essentially the I-V curve without the effects of series resistance. The original concept of the pseudo I-V curve was derived from I_{SC}-V_{OC} curves in 1963 [17]. The lumped R_S was later extracted by comparing the light I-V curve to I_{SC}-V_{OC} curve, allowing a greater understanding of ohmic power losses in solar cells [86]. By measuring the irradiance with a separate sensor cell, the I_{SC}-V_{OC} technique was later simplified to Suns-V_{OC} [87]. The independently measured light intensity is termed Suns and is used as a convenience unit describing fractions of the STC rated irradiance of 1000 W/m^2. This simple technique provided a methodology for analyzing recombination impacts on cells before and after metallization. This chapter describes the principals behind how Suns-V_{OC} works and the current applications. This information is expanded on to understand how the methodology for Suns-V_{OC} in outdoor applications, justified by means of SPICE modeling, and demonstrated with outdoor implementation.

3.1 Principals of Suns-V_{OC}

The Suns-V_{OC} methodology has been commercialized for indoor usage by Sinton Instruments with the WCT and FMT series of tools, as shown in Figure 3.1, for cells and modules, respectively [88]. The indoor testing relies on a slowly varying-intensity light source, such as a xenon bulb, which prevents unwanted heating within the test module [89]. The corresponding device's V_{OC} and operating temperature are measured alongside the

incident irradiance via an independent irradiance sensor(s). Since the test sample is under open-circuit conditions, there are no ohmic losses, resulting in a pseudo I-V curve, i.e., unaffected by R_S.

Figure 3.1. The MX Stage and WCT-120 Instrument by Sinton Instruments.

The pseudo I-V curve can be evaluated to provide electrical parameters such as pseudo fill factor (pFF), pseudo efficiency, pseudo maximum-power (pP_{MAX}), ideality factor, among others. Figure 3.2 shows an example of a Suns-V_{OC} curve used for comparison to light I-V curve, where the irradiance is expressed in "1-Suns" and the module's I_{SC} is correlated to the maximum "1- Suns" value. The difference between the voltages of the two curves can be used to calculate the R_S [90].

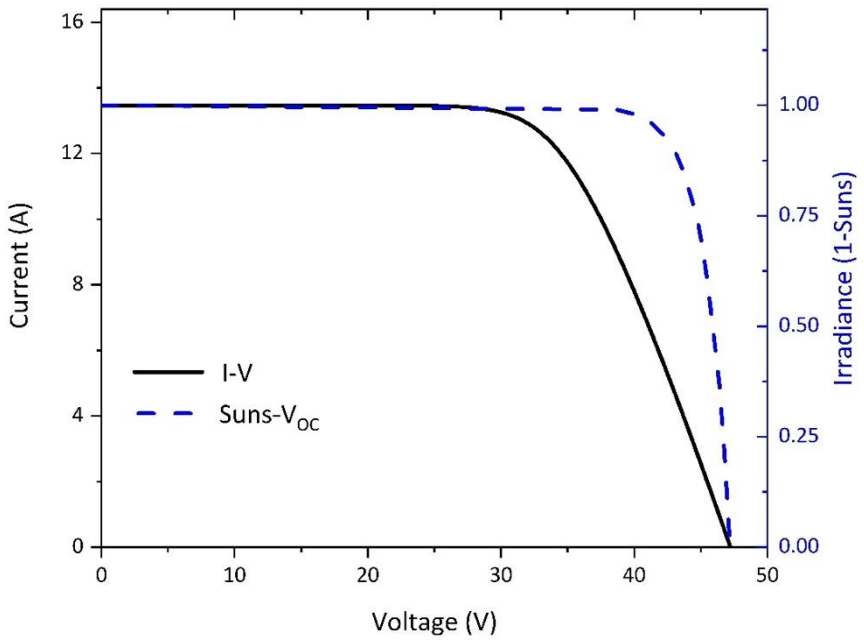

Figure 3.2. A Comparison between the I-V and Suns-V_{OC} Curves of a 72-Cell Module.

Indoor measurements benefit from the high level of control of the environmental conditions such as temperature, but there are still limitations. Roth et. al. concluded that a xenon flash could result in illumination intensity errors due to illumination inhomogeneity of the light source (up to 7.5%), spectral mismatch between test sample and irradiance sensor (up to 20%), and the height difference between sample and irradiance sensor (2.7%/cm difference in height) [91]. Additionally, inaccuracies at low injection levels may occur due to junction capacitance in high quality cells, even with a slowly changing illumination source [92]. Even with these obstacles, indoor Suns-V_{OC} characterization has been an instrumental characterization technique for several different PV technologies [93], [94].

3.2 Implementation of Outdoor Suns-V_{OC}

Suns-V_{OC} has previously been demonstrated outdoors on modules and arrays [95]–[98], but without details regarding day-to-day variation and impacts from uncontrollable weather. Variations include transient, diurnal, and seasonal effects like cloud coverage [99], temperature changes [100], wind [44], angle of incidence changes [31], spectral effects [101], albedo [102], and soiling [103]. There has recently been work that thoroughly describes the adaptation of Suns-V_{OC} for outdoor usage, measuring and normalizing for temperature and irradiance [104].

3.2.1 Suns Required at Maximum Power Point

Contrasted to indoor Suns-V_{OC}, outdoor Suns-V_{OC} takes advantage of the diurnal changes in natural solar insolation (including just before sunrise and just after sunset), providing the required changes in light intensity. The most critical point in a Suns-V_{OC} measurement corresponds to the maximum power point (M_{PP}) on the one-sun I-V curve. Since this corresponding voltage is the same in both cases, the excess carrier concentrations are roughly equivalent, even though the Suns-V_{OC} measurement is at open-circuit while the M_{PP} is under load. The equivalence in operating points means they have the same levels of recombination, and quantifying losses in the Suns-V_{OC} measurement applies directly to the I-V curve. The illumination in suns required to capture information about M_{PP}, Suns(M_{PP}), is related to one-sun I_{SC} and I_{MP} by:

$$Suns(M_{PP}) = \frac{I_{SC} - I_{MP}}{I_{SC}} \tag{13}$$

Based on the CEC database [105], the Suns(M_{PP}) for roughly 95% of commercial silicon modules falls within the range of 0.05 to 0.1 suns. Therefore, the most valuable Suns-V_{OC} data is collected during low-illumination periods of up to 0.1 suns, where the impact on system performance is nearly negligible. The Suns(M_{PP}) is likely to change slightly over time, which is a result of I_{SC} and/or I_{MP} degradation. A study of degradation rates of 12 different silicon modules found most severe I_{SC} and I_{MP} degradation of 0.71% and 0.89% annually [106]. These degradation rates correspond to a Suns(M_{PP}) increase of approximately 0.002 suns per year, or 0.05 suns over 25 years, for most modules in the CEC database. This means that outdoor Suns-V_{OC} measurements can be conducted from twilight to low irradiance conditions of 0.1 to 0.2 suns, having minimal impact on PV generation.

3.2.2 Irradiance Measurements

Measuring the irradiance is a crucial aspect to any Suns-V_{OC} measurement, indoors or outdoors. Sensors such as pyranometers can be used but may have spectral mismatch inaccuracies [107]. Though, irradiance effects, such as spectrum shifts, are of secondary importance since the V_{OC} varies with the logarithm of the light intensity [108]. To alleviate this potential issue, irradiance can be measured by monitoring the I_{SC} of a silicon solar cell positioned in-plane with the array. It has the advantage of minimizing spectral mismatch effects between the sensor and array [107], and by using similar encapsulant and glass on the sensor cell, there is assurance of similar irradiance changes from angle-of-incidence and soiling effects. The PV cell is purposely shorted with a resistor so that the output

voltage is directly proportionate to the I_{SC}. The cell must have a sufficiently high R_{SH} so that the intersecting operating point is proportionate to the I_{SC}.

The PV cell is then calibrated using an indoor steady-state light source. Indoor calibration against a reference cell gave a 99.97% coefficient of determination for the linearity of the irradiance sensor over the range of 0 to 1.2 suns as shown in Figure 3.3. Indoor Calibration of Solar Irradiance Sensor Using NREL Calibrated Cell. This calibration was validated outdoors using an NREL reference cell. The temperature dependence of the irradiance sensor is negligible due to the minor dependence of temperature on the short circuit current. The irradiance sensor is placed near the test system to minimize differences between the sensor cell and array (e.g., shadows cast on the irradiance sensor while the array is unshaded).

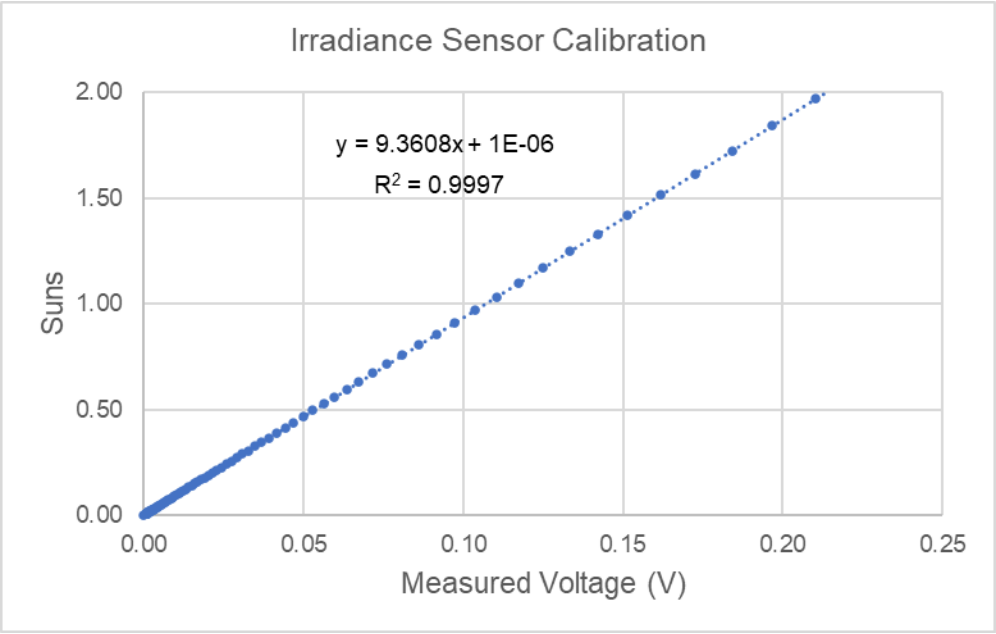

Figure 3.3. Indoor Calibration of Solar Irradiance Sensor Using NREL Calibrated Cell.

3.2.3 Temperature Measurements

The operating temperature of a PV module undergoes rapid changes during sunrise and sunset, which corresponds to the light intensities of interest. Because the open circuit voltage is highly dependent on temperature, outdoor measurements must be normalized to a specific temperature. This allows for useful comparisons between measurements, regardless of the ambient temperatures. For accurate temperature normalization, these temperature changes need to be accurately monitored, with special consideration given to the spatial distribution of module temperature. Non-uniform irradiance, wind conditions, and unmatched cell efficiencies may cause non-uniform temperature distribution[109]. In this work, temperature normalization was conducted by measuring both backsheet temperature and ambient temperatures.

Backsheet temperatures were measured by using several Texas Instruments DS18B20 temperature sensors. To compensate for spatial nonuniformity, the module backsheet temperature was taken as the average of five temperature sensors, taped to the back of the module [110]. This backsheet temperature is related to cell operating temperature using the Photovoltaic Array Performance Model [52] as:

$$T_c = T_m + \frac{E}{E_o} \times \Delta T \tag{14}$$

where T_c is the cell operating temperature, T_m is the measured back surface temperature, E is the measured solar irradiance, E_o is the reference solar irradiance (1000 W/m^2), and ΔT is the temperature difference between the back sheet and the cell at the reference irradiance. The ΔT was selected to be 3°C, based on the empirically determined coefficients found in

Table 3.1. The module type used was a glass/cell/polymer which was mounted in an open rack configuration.

Table 3.1 Empirically Determined Coefficients Used to Predict Module Back Surface Temperature as a Function of Irradiance, Ambient Temperature, and Wind Speed. Wind Speed Was Measured at the Standard Meteorological Height of 10 Meters.

Module Type	**Mount**	**a**	**b**	**ΔT (°C)**
Glass/cell/glass	Open rack	-3.47	-0.0594	3
Glass/cell/glass	Close roof mount	-2.98	-0.0471	1
Glass/cell/polymer sheet	Open rack	-3.56	-0.0750	3
Glass/cell/polymer sheet	Insulated back	-2.81	-0.0455	0
Polymer/thin film/steel	Open rack	-3.58	-0.1130	3
22X Linear Concentrator	Tracker	-3.23	-0.1300	13

The irradiance being measured is in the units of suns, which is already a ratio of the reference solar irradiance. Therefore, (14) can be simplified to:

$$T_c = T_m + Suns \times \Delta T \tag{15}$$

Measuring the backsheet temperature is only feasible for small test systems. A large array would require too many sensors for backsheet measurements to be practical. Therefore, another technique using ambient temperature was used to estimate the backsheet temperature. A local weather station measured ambient temperature and wind speed, that were then translated to backsheet temperature, based on methods also found in the Photovoltaic Array Performance Model [52]. The backsheet temperature was estimate by the following:

$$T_m = E \times e^{a+b*WS} \times T_a \tag{16}$$

where a and b are empirically determined coefficients as found in Table 3.1, WS is the measured wind speed, and T_a is the measured ambient temperature. Once the module's

back surface temperature is calculated, (15) can be used to estimate the cell's operating temperature. Chapter 3.4 later compares the results acquired by both backsheet temperature and weather station measurements.

3.2.4 Temperature Translations

Photovoltaic cells, the V_{OC} particularly, are extremely sensitive to operating temperature. When the temperature rises, the band gap of the semiconductor is reduced. This is because the energy of the electrons in the material increases with temperature. These higher energy electrons result in a reduced amount of energy to break their bonds. This reduction of bond energy results in a reduction of the band gap [111]. The open circuit voltage is most affected parameter in terms of this narrowing band gap due to temperature dependence. Therefore, temperature translations are required to ensure a benchmark for cross comparisons. In this work, the open-circuit voltage is translated to a specific temperature by the following equation [52]:

$$V_{OC(T1)} = V_{OC(T2)} - \left[M_S \times N_S \times \frac{nkT_2}{q} \times \ln(Suns)\right] - \left[M_S \times \beta_{V_{OC}(1\,sun)} \times (T_2 - T_1)\right] \quad (17)$$

where: T_1 is the translated temperature, T_2 is the measured cell temperature, M_S is the number of modules in series, N_S is the number of cells in series, n is the ideality factor, k is Boltzmann's constant, q is the electron charge, $Suns$ is the measured irradiance, and $\beta_{V_{OC}(1\,sun)}$ is the temperature coefficient for V_{OC} under full irradiance of 1 sun. When analyzing a single cell (neglecting M_S and N_S) and introducing coefficients (17) can be rewritten as [112]:

$$V_{OC} = \beta_0 + [\beta_1 \times \ln(Suns)] + [\beta_2 \times (T_2 - T_1)] \quad (18)$$

where: β_0 is the V_{OC} under 1 sun illumination at the specified temperature, β_1 is the coefficient proportionate to the thermal voltage at the specified temperature, and β_2 is the temperature coefficient of V_{OC} under fully illuminated conditions, which is assumed to be linear for all irradiance conditions.

A least squares fitting algorithm was used to perform temperature translations with independent translations performed for each day of collected data. Initial guesses for each coefficient were as follows: the module's nameplate V_{OC} value was chosen for β_0, the thermal voltage at the specified translation temperature multiplied by the total number of cells was chosen for β_1, and -0.0022 multiplied by the number of cells (change in V_{OC} per °C as calculated using empirical values for silicon) for β_2. Initial guesses are performed to enable more accurate fits. Translated results and discussion follows in Chapter 3.4.

3.2.5 Data Acquisition

The data is acquired using an AMT Mega328P microcontroller. A Texas Instruments ADS1115 provides the analog to digital data acquisition with 16 bits of resolution. This was used to enhance the resolution from the 12-bit analog input of the microcontroller. For voltages exceeding the maximum analog input of 5V, a simple voltage divider was used with high precision power resistors. The data was collected with a frequency of 5 seconds for measurements utilizing backsheet temperatures. For experiments including the weather station, the data collection frequency was changed to every 60 seconds. This change was made so the data could be correlated with the weather

station's reporting frequency. Decreasing the frequency of measurements may be conceivable, but less measurements are possible during periods of rapid irradiance changes (i.e. sunrise and sunset). Therefore, a minimum 60 second frequency is advised to ensure accurate results when translating the raw data.

3.2.6 Extraction of Suns-V_{OC} Parameters

The collected raw data is initially filtered to remove any outliers using Isolation Forest Methodology[113]. This data set is then translated to the desired temperature using procedures discussed in 3.2.4. The Suns-V_{OC} parameters are then extracted from the temperature translated data. Open-circuit voltages in this work are reported at 1 sun and 0.1 suns and can be extracted by slicing the temperature translated data at the respective irradiance value. As previously discussed, V_{OC} at approximately 0.1 suns corresponds to V_{MP} but without the effects of R_S. V_{OC} at ~0.1 suns can be directly used as a figure of merit for system performance and monitored over time. Alternately, it is possible to use the Suns-V_{OC} to extract more familiar diode parameters.

The derivative of V_{OC} with respect to the logarithm of the irradiance gives the diode ideality factor (n) as follows:

$$n = \frac{q}{kT} \frac{d\, V_{OC}}{d\, \ln(suns)} \tag{19}$$

While n is be presented as a curve [114], the most relevant metric for performance analysis is from 1 sun V_{OC} to 0.1 suns (corresponding to M_{PP}). Taking the slope from 0.1 to 1 $suns$ also has the advantage of being less affected by noise than the tangent. Further

analysis gives pP_{MP} and pFF, which are the maximum power point and fill factor respectively, in the absence of R_S. The pP_{MP} can be estimated by equating suns to the system I_{SC} as follows:

$$pP_{MP} = [(1 - suns) \times I_{SC} \times V_{OC}]_{max} \tag{20}$$

For high resolution Suns-V_{OC} data, pFF can be calculated as:

$$pFF = \frac{[(1-suns) \times V_{OC}]_{max}}{V_{OC(0.1\ suns)}} \tag{21}$$

However, outdoor field data typically has insufficient resolution to determine the maximum accurately, so we use n from equation (19) to empirically estimate pFF using both equation (22) and equation (23) [115]:

$$pFF = \frac{\nu_{OC} - \ln(\nu_{OC} + 0.72)}{\nu_{OC} + 1} \tag{22}$$

$$\nu_{OC} = \frac{q}{nkT} V_{OC} \tag{23}$$

These two equations also assume a single ideality factor from V_{OC} to M_{PP} and we can use the previously calculated value of n. The approximation assumes that the series resistance is zero and that the shunt resistance is infinite. Therefore, modules with shunting issues may not yield accurate pFF approximations. Another exception is due to the complexity of the ideality factor and the relationship to operating voltage. Inaccurate determination of ideality factor, or heavy reliance on a single point also yields inaccuracies when using this pFF approximation [116].

3.3 Suns-V_{OC} Modeling

Shading of PV complicates the analysis of module and array I-V curves. Bypass diodes create "stepped" I-V curves in partial shade; these stepped curves are typically filtered out when performing long-term analysis on large I-V curve datasets [117]. Circuit modeling, using LTspice (Linear Technology Corp), is conducted to demonstrate the stability of Suns-V_{OC} curves obtained from varying partial shade conditions that would otherwise generate erratic stepped I-V curves [118].

A model was built of a three-string, 96-cell solar module comparable to those used in outdoor experimentation as shown in Figure 3.4. Individual PV cells were simulated based on a single-diode model, using R_S and R_{SH} values of 0.01 Ω and 300 Ω, respectively [119]. For Suns-V_{OC} measurements, the open-circuit voltage was measured as the light generated current was swept from 0 to 1 sun, with no load across the module. For Light I-V measurements, the voltage was swept from 0 to V_{OC} while measuring the respective current.

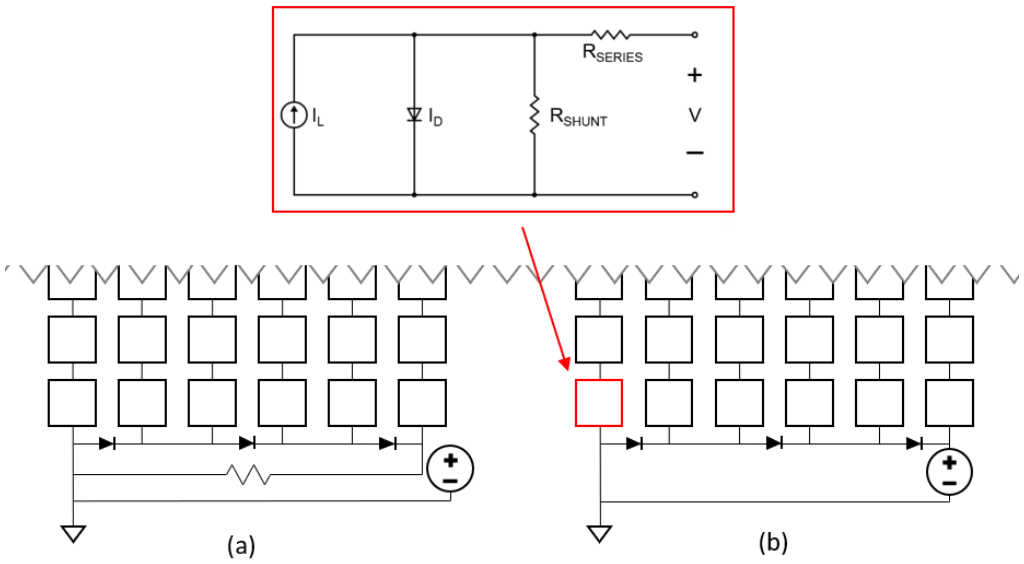

Figure 3.4. LTspice Circuit Model of a 96-cell PV Module for (a) Suns-V_{OC} and (b) Light I-V analysis.

Both I-V and Suns-V_{OC} measurements were simulated with various shading scenarios. Figure 3.5 shows modeled light I-V and Suns-V_{OC} curves for one sun irradiance with 50% partial shading affecting one, two, and three cells, each from a different string. The incident irradiance for the Suns-V_{OC} simulation is plotted as 1-Suns, so that the results are easily comparable to the light I-V results.

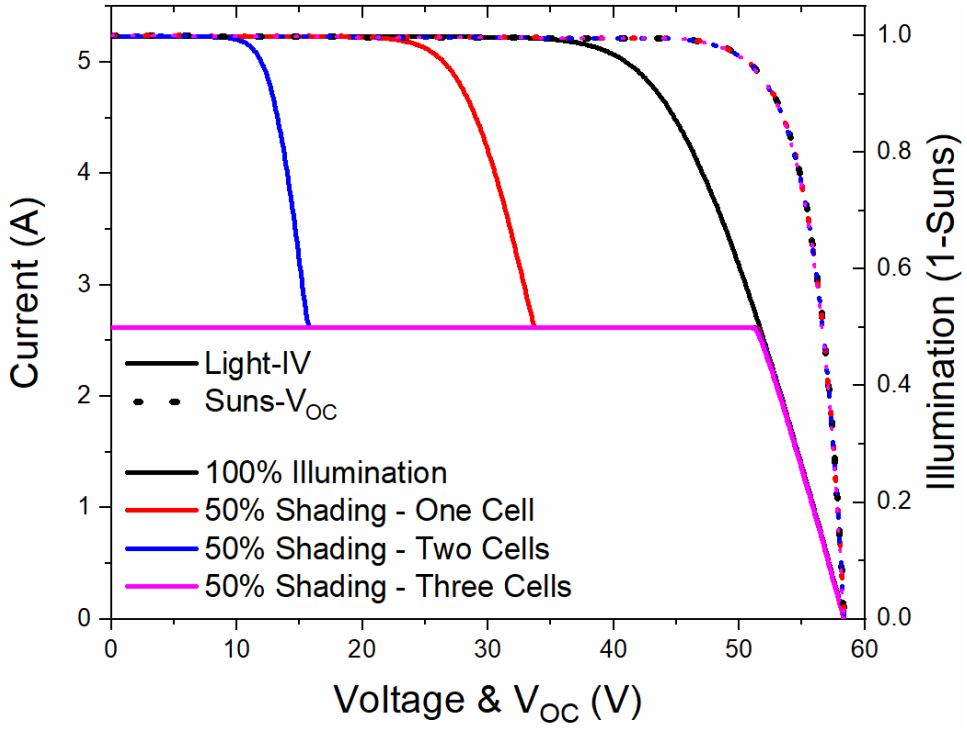

Figure 3.5. Simulated Shading Impacts on Light I-V and Suns-V_{OC} Curves.

The difference between the I-V and Suns-V_{OC} curves with zero shading is the manifestation of R_S. The steps found within the shaded simulations for the light I-V curve represent the activation of the bypass diodes. The bypass diodes only minimally impact the Suns-V_{OC} curves. When comparing the fully illuminated model to that of the three shaded cells, the pP_{MP} dropped by 0.2%, whereas the light I-V P_{MP} dropped by 35.5%.

To further explore the stability of Suns-V_{OC} in widely varying partial shade conditions, the 96-cell module LTspice model is extended to include many different partial shading scenarios. These scenarios were created to demonstrate a wide range of possible partial shade conditions but are not necessarily reflective of real-world partial shading for a typical system. Figure 3.6 shows frequency histograms of the P_{MP} from I-V and pP_{MP} from Suns-V_{OC}, from roughly 500 unique partial shade scenarios. Scenarios include

shading affecting two of the three strings, from 0% (completely shaded) to 100% (fully illuminated), whereas string three is held at fully illuminated conditions. The x-axis of Figure 3.6 corresponds to the shading level on the most shaded of the three strings.

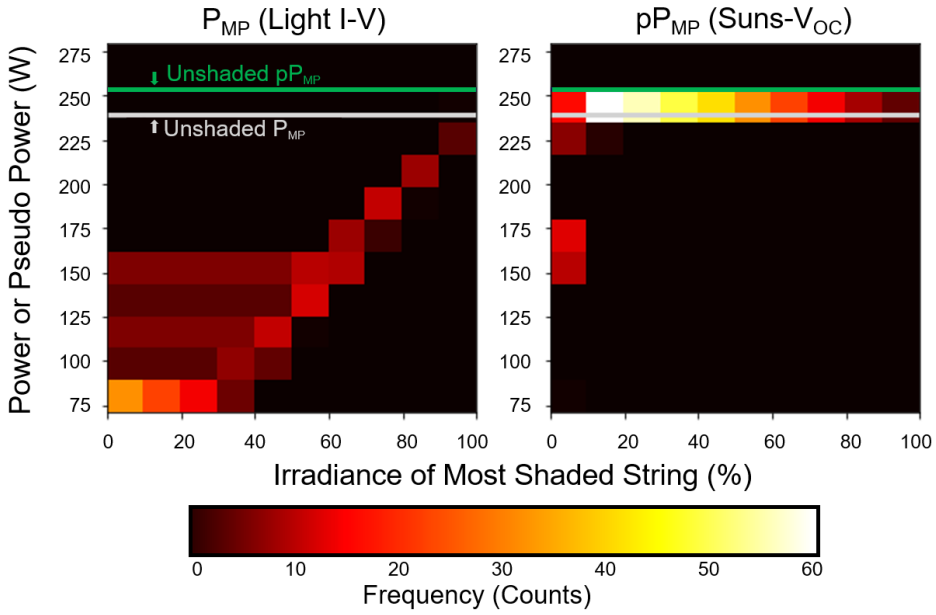

Figure 3.6. Frequency Histogram Displaying Maximum Power (Light I-V) and Pseudo Maximum Power (Suns-V_{OC}) of a 3-String 96-Cell Module, Using ~500 Different Partial Shading Conditions. String 1 and 2 are Independently Shaded from 0 to 100% Illumination. String 3 is Maintained at 100% Illumination.

As seen on the left side of Figure 3.6, P_{MP} varies substantially due to bypass diode activation and reduced light-generated current. For the given shading scenarios, the average of P_{MP} is 126 W with a standard deviation of 40.5 W. The right half of Fig. 3 shows that Suns-V_{OC} pP_{MP} falls within a much more tightly distributed range, with an average of 238 W and a standard deviation of 25.7 W. Suns-V_{OC} provides a pP_{MP} within approximately 5% of the unshaded pP_{MP} when all strings are illuminated at values greater than ~5%. These results suggest that in systems that regularly operate in partial shade, I-V curves, or time-series P_{MP} data might rarely contain useful diagnostic information. Considering diffused

irradiance is typically well over 5% of total illumination [120], scenarios of less than 5% absolute illumination anywhere on the module are rare, even during periods of major shading. While true pP_{MP} requires uniform irradiance, a close estimate of pP_{MP} is obtained under almost all irradiance and shading conditions. Suns-V_{OC} curves frequently provide a value of pP_{MP} within 5% of the true unshaded pP_{MP}, providing a basis for robust time-series performance monitoring.

3.4 SUNS-V_{OC} EXPERIMENTAL

This chapter explains the experimental work performed using outdoor Suns-V_{OC}, as outlined in [104]. Testing was performed in Tempe, Arizona, USA; test PV was ground mounted, facing due south at a 33° tilt angle. Initial experiments were conducted on single-cell modules both indoors and outdoors. Subsequent testing was then performed on a 96-cell module and then a 4-module array.

3.4.1 Single Cell Validation Testing

The preliminary testing utilized a single-cell module encapsulated within ASU Solar Power Labs. The module was packaged in a ~413 cm^2 square footprint with a low iron glass front sheet, ethylene vinyl acetate (EVA) encapsulation, and a white polyvinylidene fluoride (PVDF) backsheet. The cells used were 156 mm pseudo square monocrystalline silicon with back surface field (BSF) architecture. Single-cell modules were used because measurements could be validated using an indoor Suns-V_{OC} tester.

The single-cell module was placed outdoors and measured continuously as described in chapter 3.2. The raw data collected for six days is displayed in Figure 3.7, which consists of backsheet temperature, operating temperature as calculated in (15), incident irradiance, and open-circuit voltage.

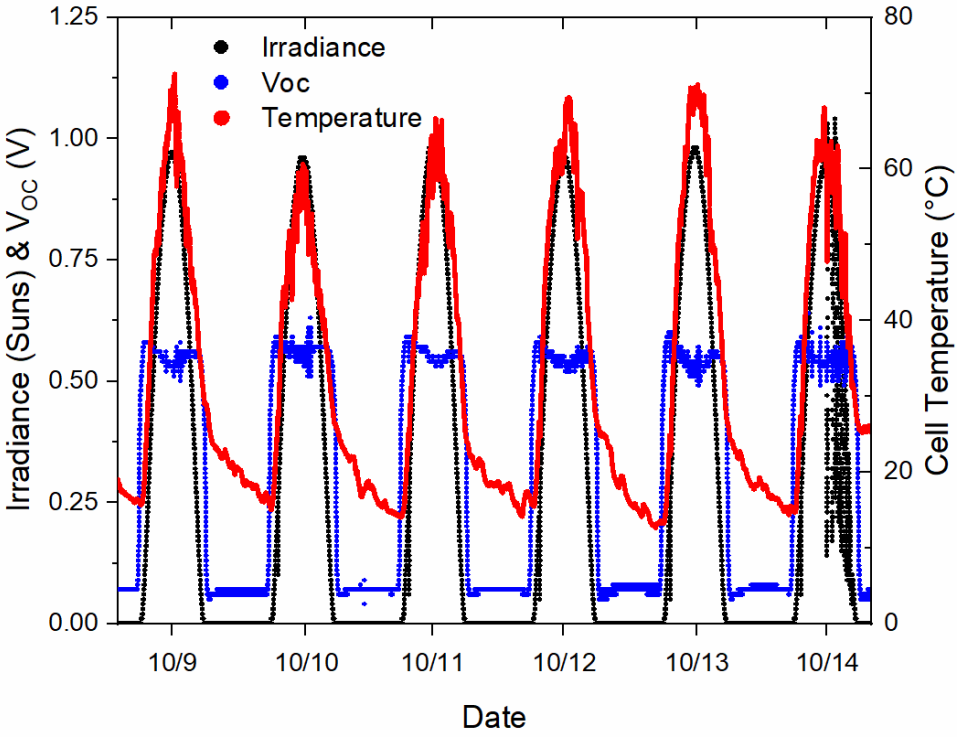

Figure 3.7. Raw Data for Outdoor Suns-V_{OC} on a Single-Cell Module.

The data plotted for a single cell in Figure 3.7 is primarily full of clear sky days with the last day of data collection consisting of intermittent cloud coverage. The entire dataset was used for further analysis. The open circuit voltage never gets to 0V, which is possibly noise from the DAQ. Another explanation for the open circuit voltage not going to 0 is the moon phase during this period of testing. On October 13th, 2019, there was a full moon meaning the low irradiance of 2.5 µW could potentially increase the open circuit

voltage. With that being said, the open-circuit voltage never goes to zero, meaning the effect of moonlight was unlikely the cause for not reading zero.

The raw data was then normalized to different temperatures using the equations outlined in (18). A few different temperatures were chosen to normalize the data to; 10 °C, 25 °C, and 40 °C. Temperatures of 25 °C are used for STC measurements, whereas 10 °C and 40 °C are used to demonstrate translations to lower and higher operating temperatures. The theory was to ensure that the temperature translations would be feasible when translating to temperatures with greater deltas from the actual operating temperature. The same cell was then measured indoors by using a Sinton FCT-450 cell flash tester at these same respective temperatures. To achieve a temperature of 10 °C, the module was placed into a freezer and then measured. The higher temperature of 40 °C was measured after placing the module in a muffle furnace, where it was slowly heated to the appropriate temperature. The outdoor temperature translated Suns-V_{OC} curves are displayed in Figure 3.8 with the corresponding indoor measurement results.

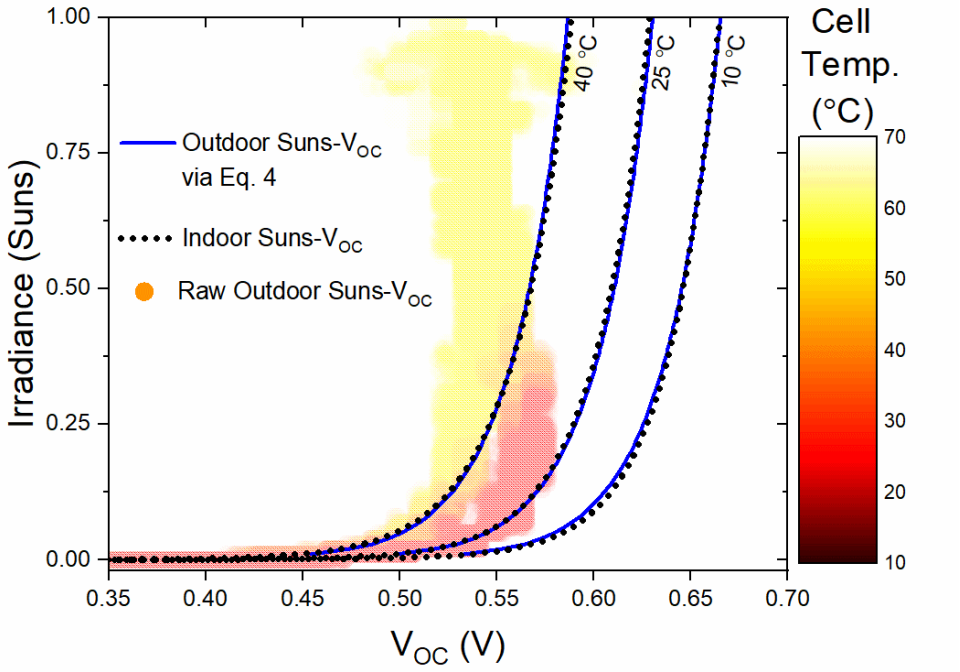

Figure 3.8. Temperature Translated Outdoor Suns-V_{OC} Compared to Indoor Suns-V_{OC} on Single-Cell Module [104].

The measured V_{OC} datapoints are colored by cell temperature as determined from backsheet temperature measurements and (15). When inspecting the raw data, there is a wide variation in V_{OC} when above 0.9 suns. This is due to the difference in temperatures during early noon as compared to late evening. In early morning, the cells are still relatively cool, but during early evening (at the same irradiance), the cells have a much hotter operating temperature. There may also be some variation from nonuniform temperature. The temperature translated results are graphed in the blue line plot, while the respective indoor results are graphed with the black dotted line plot. Normalizing the measured outdoor data via (18) to 10 °C, 25 °C, and 40 °C, yields an excellent agreement with the

indoor measurements. The Suns-V_{OC} parameters for each outdoor temperature translation are shown in Table III, with the respective indoor parameters at the same temperature.

Table 3.2. Suns-V_{OC} Parameters on a Single-Cell Module for Both Indoor and Normalized Outdoor Measurements.

Temperature (°C)	**Indoor/Outdoor**	**R_S (Ω-cm^2)**	**V_{OC} at 1 Sun (V)**	**V_{OC} at 0.1 Suns (V)**	**n**	**pFF**	**pP_{MP} (W)**
10	Indoor	2.89	0.665	0.603	1	0.834	4.71
	Outdoor	2.72	0.665	0.599	1.02	0.831	4.7
25	Indoor	2.95	0.629	0.563	1.11	0.821	4.39
	Outdoor	2.96	0.63	0.564	1.12	0.82	4.39
40	Indoor	3.01	0.589	0.519	1.27	0.803	4.02
	Outdoor	3.02	0.587	0.52	1.25	0.806	4.02

The indoor and outdoor compared series resistances have larger discrepancies at low temperatures, though as expected, both increase as a function of temperature. The pP_{MP} values of the temperature-translated outdoor Suns-V_{OC} curves are within 0.04% (relative) of the respective indoor Suns-V_{OC} curves for 25 °C and 40 °C, indicating the validity of the outdoor measurement setup and V_{OC} translations via (18). A slightly larger percentage difference of 0.2% (relative) occurs for the pP_{MP} values when translating to 10 °C. This is likely due to the paucity of data at such low temperatures for generating fit coefficients, considering the average outdoor operating temperature was approximately 35 °C. This becomes more obvious when looking at the relative percentage difference in ideality factors, which is 2% different at 10 °C. Translating data to temperatures closer to the average operating temperature results in a more accurate fit. The specified translation temperature is best chosen given the average operating temperature of a given site or season.

The measurement error when comparing outdoor to indoor measurements must be less than the percentage of expected degradation to ensure viability. Modules are typically warrantied for ~1% degradation of maximum power per year. The measurement error for outdoor compared to indoor measurements equate to less than 0.04% error for pP_{MP}, when analyzing using 25 °C and 40 °C for temperature translations. Because the measurement error is significantly less than the typical warrantied degradation, one should be able to use this data to make a reasonable assumption regarding rates of degradation.

3.4.2 Single Module Validation Testing

Outdoor Suns V_{OC} was validated at the cell level in Chapter 3.4.1. The next step was to prove the feasibility using a representative industry module. The module used is a 3-string, 96-cell monocrystalline silicon Plurigas Solar Energias model BSM230. This module is similar to the module simulated in Chapter 3.3. Datasheet standard test condition (STC) (AM1.5G, 25 °C, 1000 W/m^2) ratings of the panels are found in Table 3.3. The history of these modules is not completely known, but these modules had been in the field for at least 5 years while under open circuit conditions.

Table 3.3. STC Ratings of BSM230 PV Modules.

Parameter	Value
P_{MP}	230 (± 5%) W
I_{MP}	4.82 (± 5%) A
V_{MP}	48.05 (± 5%) V
I_{SC}	5.23 (± 5%) A
V_{OC}	58.6 (± 5%) V

A single module was measured using the methodology outlined in Chapter 3.2. The data was collected during winter (February) and autumn (September). A snippet of this data from both seasons is shown in Figure 3.9. The data includes irradiance, cell temperature, and measured V_{OC}.

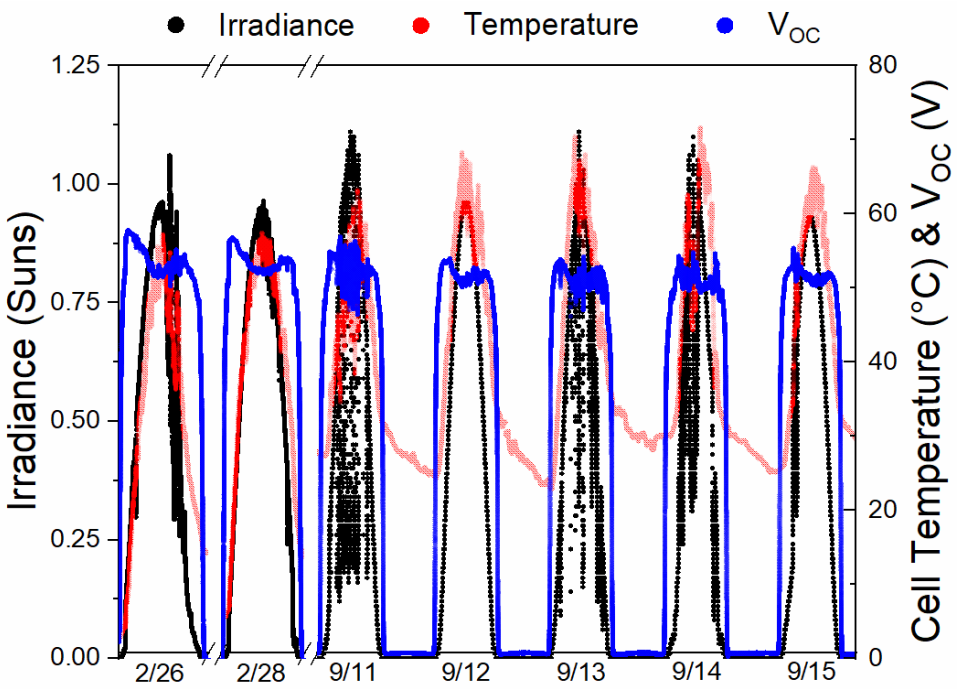

Figure 3.9. Solar Irradiance, Cell Temperature, and Measured V_{OC}, for a 96-Cell PV Module Located in Tempe, AZ, USA During February and September of 2019.

The seasonal impact of this data can be seen in several different ways. The irradiance during the autumn season is about 20% higher than the irradiance during the winter. This irradiance impact is expected due to the tilt angle and geographic location used for testing. The cell temperature is also higher during the autumn months, with a relative increase by about 25%. This can also be seen in the reduced open circuit voltages graphed in September as compared to those graphed in February. A final observation is the scattered cloud coverage, as seen in the irradiance in the autumn months. Each day was analyzed

independently to quantify the variation introduced by these daily and seasonal weather changes. The Suns-V_{OC} curves are displayed in Figure 3.10, using a temperature translation of 40 °C.

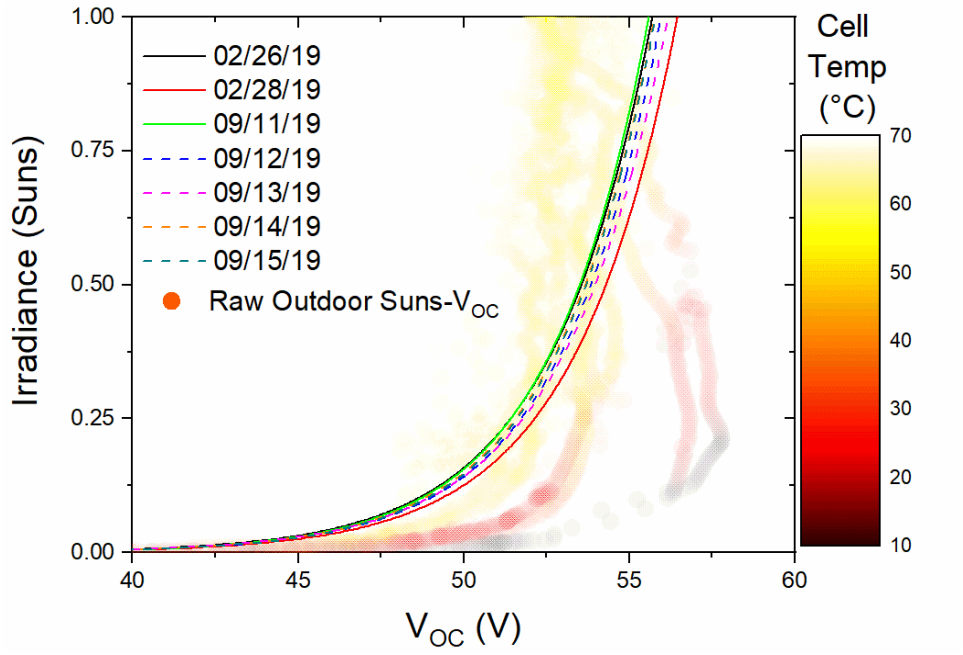

Figure 3.10. Outdoor Suns-V_{OC} Curves Translated to 40 °C for a 96-Cell Module, Comparing Seasonal and Daily Changes [104].

The raw data displayed in Figure 3.10 is colored based on the cell temperature derived from 5 backsheet temperatures. Because of the seasonal effect, there are major differences in voltage output and corresponding temperatures. Open circuit voltages are as high as 58V at approximately 10 °C and as low as 52V at approximately 70 °C. The data was then translated to 40 °C, but earlier results displayed in Table 3.2 show that translations far from actual operating temperatures may potentially induce larger errors. This becomes evident when looking at the single Suns-V_{OC} curve for February 28, 2019. There is a noticeable deviation from the grouping as seen in the Suns-V_{OC} parameters in Table 3.4.

Table 3.4. Suns-V_{OC} Parameters on a 96-Cell Module Using Full Day of Irradiance Data.

Date	Avg. Cell Temp. (°C)	V_{OC} at 1 Sun (V)	V_{OC} at 0.1 Suns (V)	n	pFF	pP_{MP} (W)
2/26/2020	32.8	55.69	48.58	1.19	0.809	235.7
2/28/2020	34.9	56.46	49.29	1.20	0.809	238.9
9/11/2019	43.6	55.59	48.67	1.16	0.812	236.1
9/12/2019	49.5	55.96	48.92	1.18	0.811	237.4
9/13/2019	49.3	56.16	48.88	1.22	0.807	237.0
9/14/2019	46.3	55.76	48.78	1.22	0.811	236.5
9/15/2019	48.1	55.79	48.83	1.16	0.812	236.9

Assuming the module had negligible degradation over this six-month period, each day's respective translated Suns-V_{OC} curve should be similar. Daily pP_{MP} values obtained across these days are listed in Table IV and are within 1.3% of each other. Daily variations are roughly equal in magnitude to seasonal variations, indicating that the methodology is robust to seasonal weather variation. The results show that for daily changes, there is minimal variability when comparing the February data to the September data. The seasonal temperature extremes may cause the subtle differences found between seasons. September temperatures were approximately an average of 10 to 15 °C warmer than February. Because the temperature translations were to 40 °C, there is more variability in the spring weather, where the average operating temperature was cooler.

For practicability, a characterization technique on a large system must not interfere with normal power production. Potentially, Suns-V_{OC} data can be collected only during low irradiance periods at sunrise and sunset. Testing this hypothesis, the individual daily data displayed in Figure 3.9 was also analyzed while only considering data collected during sunrise and sunset (irradiance values <150 W/m^2). The resulting Suns-V_{OC} curves for using only low irradiance data are displayed below in Figure 3.11; the full irradiance results from

February 28th and September 11th in Figure 3.10 are also displayed for reference. The x-axis has been zoomed in and the raw data was removed to help distinguish between the different datasets.

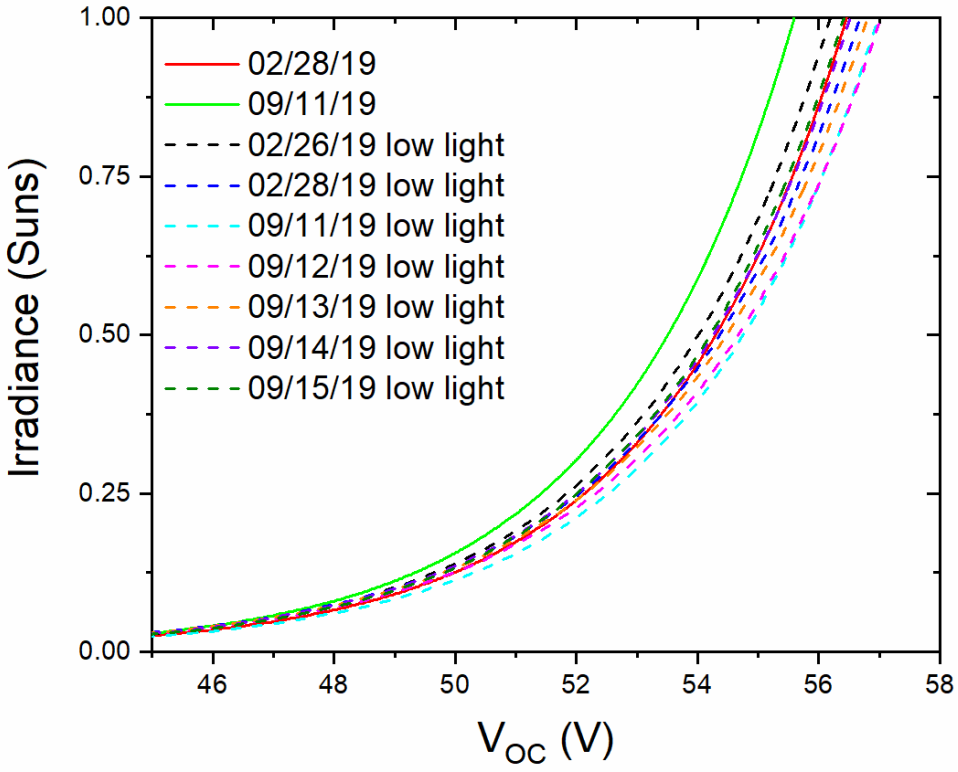

Figure 3.11. Outdoor Suns-V_{OC} Curves Translated to 40 °C for a 96-Cell Module, Comparing Low Irradiance Datasets vs. Full Irradiance Datasets.

Similar variability is observed when comparing full-day data to sunrise and sunset limited data. Temperature translations may also play a role in these differences; operating temperatures during low light intensity in the morning and evening are lower than the overall average operating temperature. The resulting Suns-V_{OC} parameters are displayed in Table 3.5.

Table 3.5. Suns-V_{OC} Parameters on a 96-Cell Module Using Only Low Irradiance Data of Less than 150 W/m^2. Percent Differences Are Compared to Full Irradiance Data as Shown in Table 3.4.

Date	V_{OC} at 1 Sun		V_{OC} at 0.1 Suns		n		pFF		pP_{MP}	
	(V)	% Diff	(V)	% Diff	n	% Diff	pFF	% Diff	W	% Diff
2/26/2020	56.19	0.89	48.96	0.78	1.21	1.65	0.807	-0.25	237	0.63
2/28/2020	56.98	0.91	49.59	0.60	1.21	0.83	0.809	-0.37	240	0.54
9/11/2019	56.68	1.92	48.99	0.65	1.29	10.08	0.800	-1.50	237	0.42
9/12/2019	57.02	1.86	49.21	0.59	1.29	8.53	0.801	-1.50	238	0.38
9/13/2019	56.80	1.13	49.06	0.37	1.30	6.15	0.800	-0.88	238	0.29
9/14/2019	56.52	1.34	49.01	0.47	1.30	6.15	0.799	-1.00	237	0.38
9/15/2019	56.41	1.10	49.09	0.53	1.23	5.69	0.806	-0.74	238	0.38

The discrepancies between using data from the full day and only periods of low illumination are consistent from day-to-day, with relative average changes of 0.5% for V_{OC} at 0.1 suns, -0.9% for pFF, and 0.4% for pP_{MP}. There can be much larger variations in V_{OC} at 1 sun, due to omission of data at that light intensity. There are also larger variations in ideality factor, which is likely due to the extreme temperature sensitivity. Methodology should remain consistent to ensure parameters are analogous (e.g., low illumination only). These results suggest that Suns-V_{OC} data collected daily, during periods of low illumination, resulted in stable metrics within a 1% range of variation. Analyzing longer time periods, such as weekly or monthly, averages out any day-to-day noise. True power measurements may have daily variances on the order of 10% to 20%, where Suns-V_{OC} measurements are much more tightly distributed.

The data analyzed thus far has all used multiple temperature sensors attached to the backsheet and irradiance sensors positioned in-plane, close to the modules. This method is unrealistic when considering larger systems, where replacing temperature and irradiance sensors with on-site weather station data is an alternative. Temperature translations on a

96-cell module were compared using both backsheet temperature sensors and local weather station data that included pyranometer plane-of-array (POA) irradiance, wind speed, and ambient air temperature. The cell temperature from the weather station data was calculated using (16). Two days in March were used to compare measured backsheet temperature data with data captured from an on-site weather station. The weather station was positioned ~10 m away from the module, capturing data at a frequency of one minute. Weather station sensors were ~2 m off the ground, where modules and their respective local sensors were ground mounted. When analyzing Suns-V_{OC} using weather station data, the weather station POA irradiance was used instead of the local irradiance sensor. The resulting temperature comparisons are displayed in Figure 3.12.

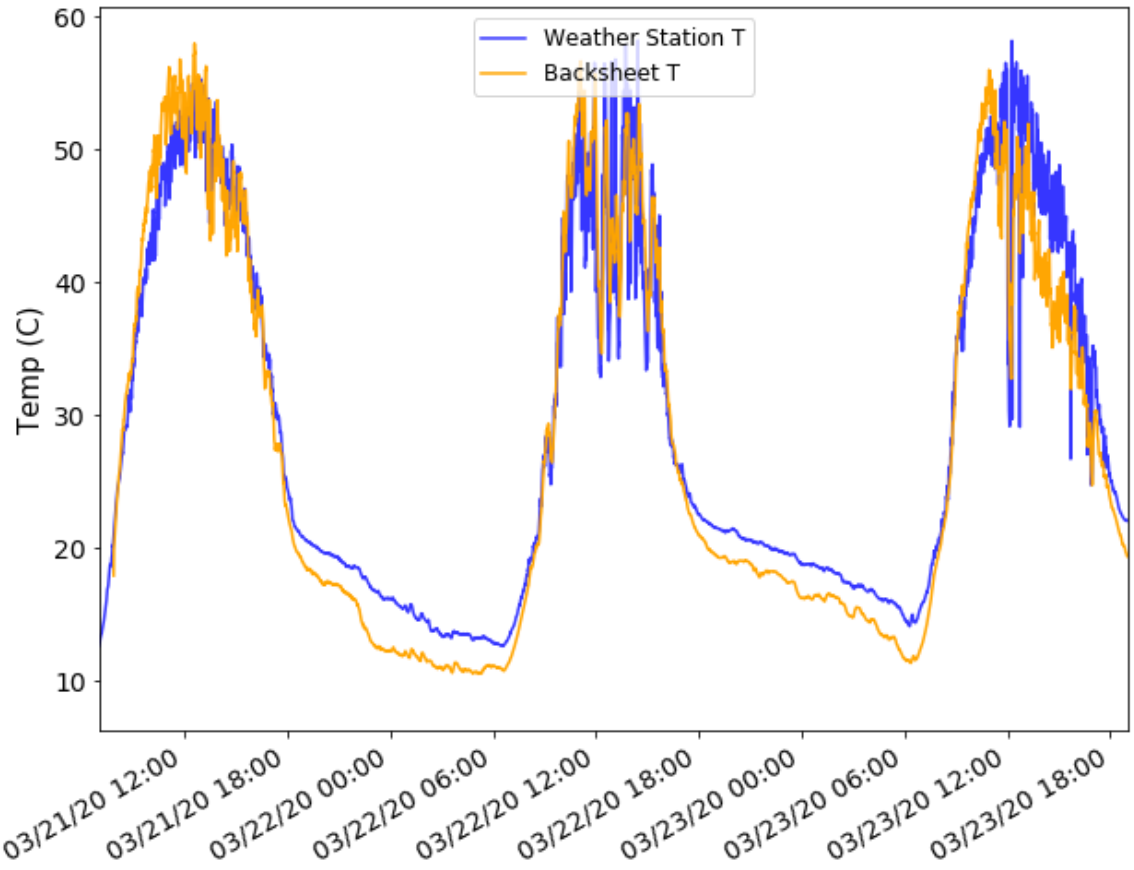

Figure 3.12. Cell Temperature of a 96-Cell PV Module Calculated via (16) Using a Weather Station and Compared to Measured Backsheet Temperature.

The orange curve represents the cell temperature as calculated from the local backsheet temperatures, whereas the blue curve represents the cell temperature as calculated from the weather station data. The periods during night hours have larger deltas, but this is just an artifact of the difference between air temperature and the temperature of the back of the modules. The two methodologies were then used to create Suns-V_{OC} curves, translated to 40 °C, which are displayed in Figure 3.13.

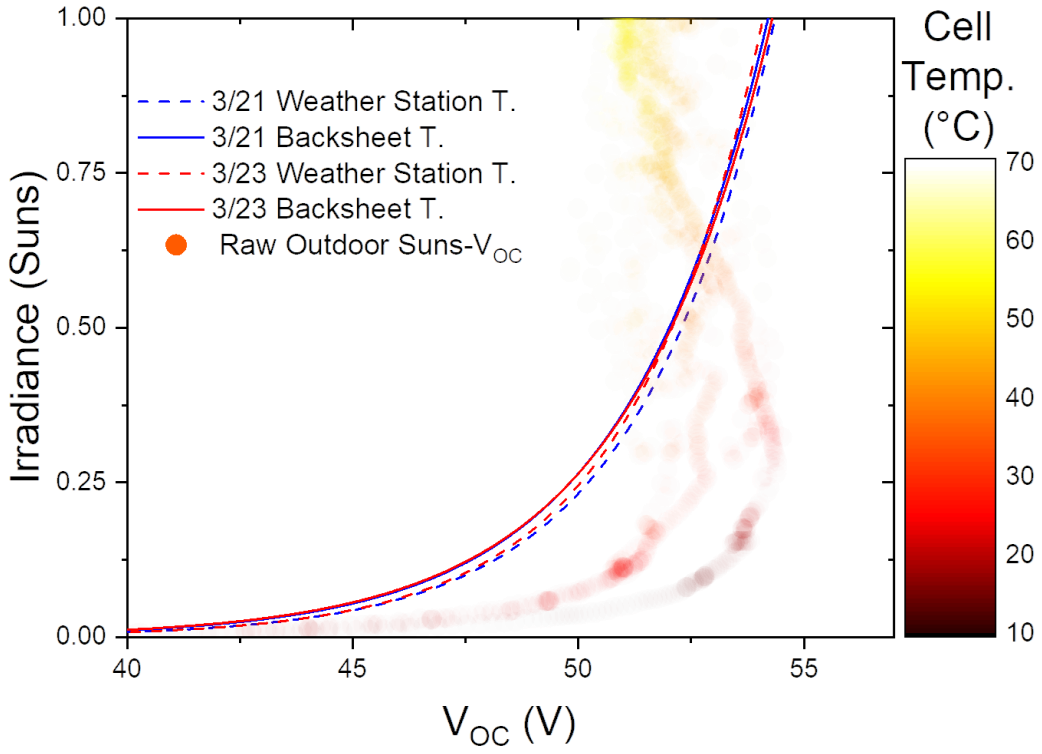

Figure 3.13. Suns-V_{OC} Curves Translated to 40 °C for a 96-Cell Module Using Measured Backsheet Temperature and Weather Station Data.

The results show slight inconsistencies during periods of low illumination, when using measured backsheet temperature compared to the weather station data. Using weather station data yields results in Suns-V_{OC} curve translations within ±1% of the backsheet sensor translations. The largest differences occur in periods of low illumination. This is suspected to be due to rapid changes in operating temperature during low irradiance periods. Table 3.6 displays the Suns-V_{OC} parameters, highlighting the slight discrepancies.

Table 3.6. Suns-V_{OC} Parameters on a 96-Cell Module Using Measured Backsheet Temperature Vs. Weather Station Data.

		V_{OC} at 1 Sun (V)	**pFF**	**pP_{MP} (W)**
3/21/2020	Backsheet	54.20	0.802	227.3
	Weather Station	54.36	0.807	229.4
3/23/2020	Backsheet	54.30	0.800	227.2
	Weather Station	54.10	0.806	228.1

The variability found when comparing localized sensors to more broad data, such as weather stations, may be vulnerable to site specific nuances. For example, the location of this experiment was placed next to the side of a large building. This building blocks a significant portion of wind, as shown in Figure 3.14. It is very rare for wind to blow in the North/South direction for this specific location. The weather station is located more towards the corner of the building, which means it may measure wind that isn't affecting the PV modules.

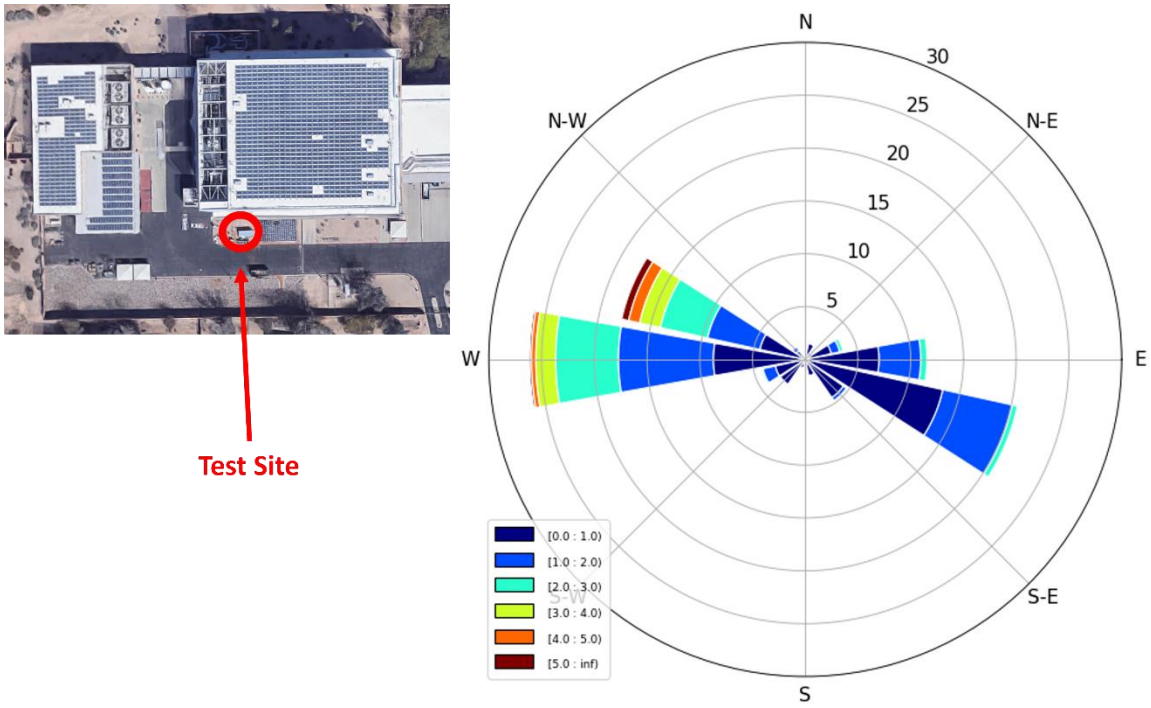

Figure 3.14. A Wind Rose Showing the Percentage of Wind Gusts, the Magnitude, and the Direction for Weather Station Site Data Collected on March 21-23.

Another factor that can severely impact the weather station data is how the empirical coefficients (a and b) used in (16) are determined. According to [52], a ranged from -2.81 to -3.58 and b ranged from -0.0594 to -1.3. Using the data from Figure 3.12, these empirical coefficients were slightly adjusted to examine the sensitivity of their impact. The resulting impact is overlayed and displayed in Figure 3.15. The blue curve is based on the coefficients used in this study. The dramatic change in the a coefficient greatly increased the upper limit, whereas the change in the b coefficient changes the rate of cooling.

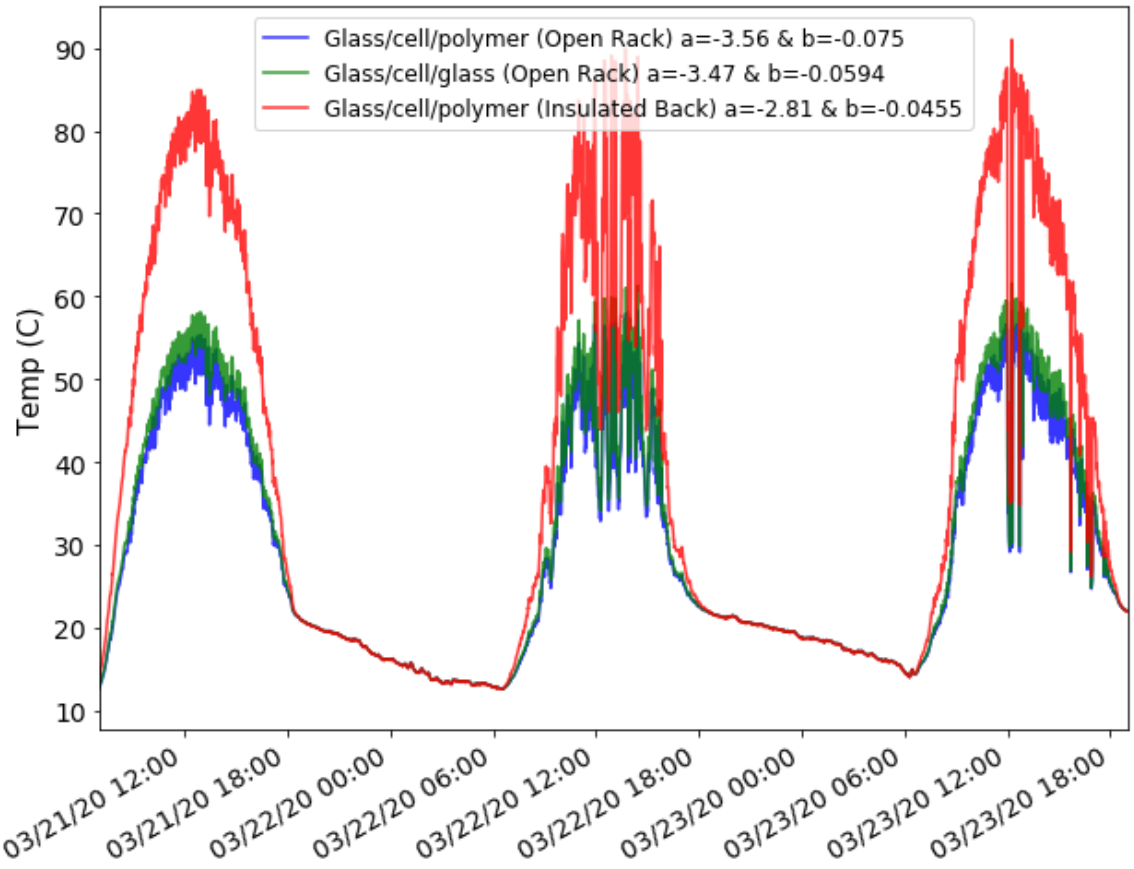

Figure 3.15. Cell Temperature Comparison of a 96-Cell PV Module Calculated via (16) Using Different Configurations of a and b.

Results demonstrate that V_{OC} and pFF are in good agreement when comparing the values obtained from measured backsheet temperature to those gathered exclusively using weather station data. In situations regarding large PV power plants, where implementation of individual temperature sensors is unrealistic, weather station data can be used to estimate the module's operating temperature. Based on this analysis, it is highly recommended that coefficients be empirically determined for the respective system and location. Overall, across variations in day and season, with or without limiting data to low irradiance

conditions, and using only on-site weather station data, Suns-V_{OC} results in stable metrics within a ± 1-2% range of variation.

3.4.3 Array Outdoor Testing

PV arrays are an assembly of PV modules connected in a system with one output. Modules are rarely used independently outside of an array. Therefore, Suns-V_{OC} testing was conducted on a small array, comprised of the same modules as outline in Table 3.3, to provide an example of feasibility. A four-module array was analyzed in March 2020 for six days under split conditions. The first three days monitored the array's V_{OC} under unshaded conditions. For the last three days, one single module was artificially shaded at approximately 50% illumination by applying an opaque sheet on top of the surface of the module. Each module had three temperature sensors, totaling twelve sensors for the array. The irradiance was measured using a single irradiance sensor ~1 m from the array. The measured irradiance, operating temperature, and raw V_{OC} are displayed in Figure 3.16.

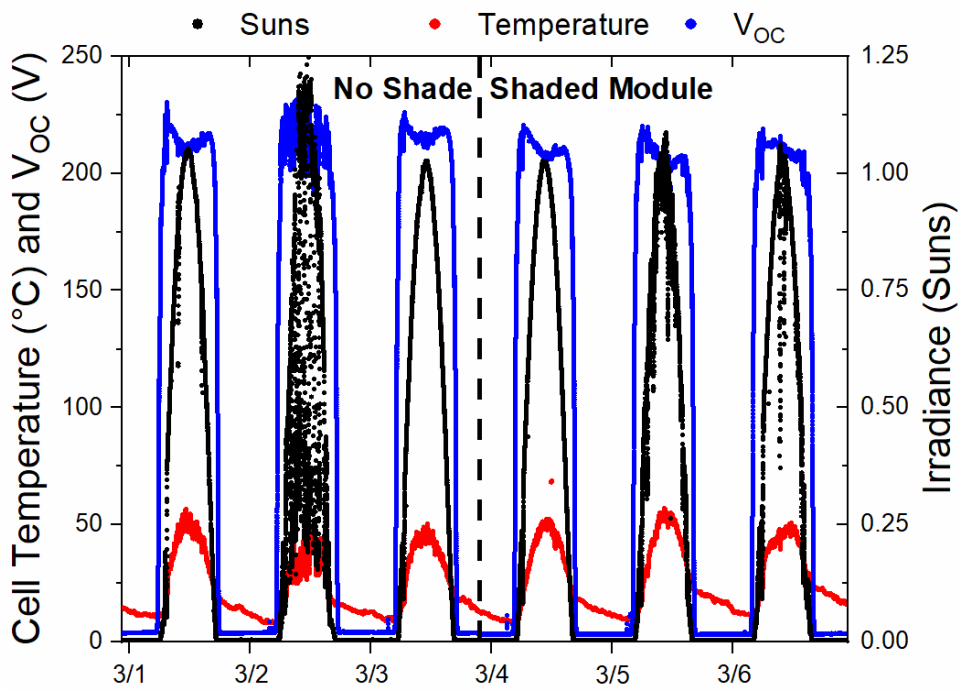

Figure 3.16. Solar Irradiance, Operating Temperature, and Measured V_{OC}, for a 4-Module Array with Both Full Illumination and 50% Partial Shading on a Single Module.

The results shown in Figure 3.16 are split between days with no shading (March 1st to March 3rd) and days with intentional shading on a single module (March 4th to March 6th). There is intermittent cloud coverage on March 2nd and March 6th. The more severe cloud coverage on March 2nd results in an elevated irradiance and corresponding V_{OC}, due to cloud enhancement increasing the diffused component of irradiance [121]. The resulting Suns-V_{OC} curves of the array are displayed in Figure 3.17 for each day and translated to 40 °C. Each day was independently analyzed, to determine the resilience of shading effects on Suns-V_{OC}.

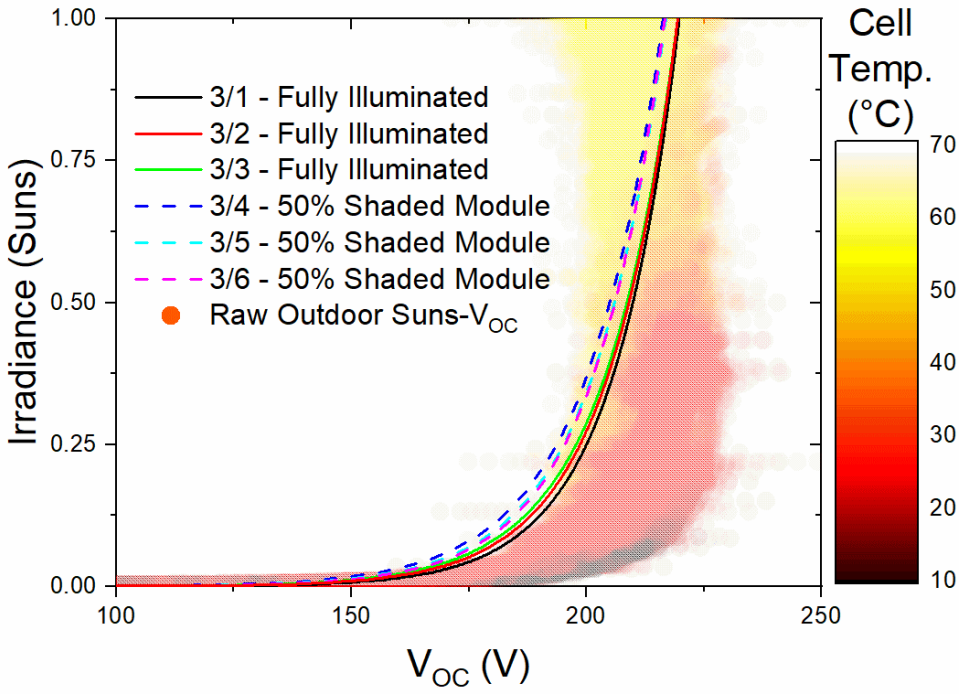

Figure 3.17. Outdoor Suns-V_{OC} Curves of a 4-module Array Under Normal Illumination Conditions and a 4-Module Array with One Shaded Module at 50% Illumination Conditions. March 1st to March 3rd Are Under Normal Illumination Conditions. March 4th to March 6th Are Under Shaded Illumination Conditions.

There is good agreement of the resulting Suns-V_{OC} curves between the three days of each respective split. When comparing the unshaded results to the shaded module results, there is a slight decrease in V_{OC}. This agrees with LTspice simulations, which suggest a 2-3 V drop in V_{OC} when applying 50-60% shading. The Suns-V_{OC} parameters for each day are found in Table 3.7.

Table 3.7. Suns-V_{OC} Parameters on a 4-Module Array with Full Illumination Vs. ~50% Shading on a Single Module.

Illumination Conditions	**Date**	**V_{OC} at 1 Sun (V)**	**n**	**pFF**
100% Illumination	3/1/2020	219.73	1.373	0.766
	3/2/2020	219.41	1.373	0.766
	3/3/2020	219.41	1.373	0.765
~50% Shading on Single Module	3/4/2020	216.30	1.373	0.764
	3/5/2020	216.86	1.373	0.764
	3/6/2020	216.64	1.373	0.764

The extracted Suns-V_{OC} parameters are almost identical for the three-day splits. When comparing unshaded to shaded conditions, there is a noticeable, but expected drop in V_{OC}. The average delta in V_{OC} is 2.9 V, which equates to a 3 mV drop in V_{OC} for each cell in the shaded module. The ideality factor and pseudo fill factor are almost identical. These results suggest that Suns-V_{OC} is resilient to significant levels of partial shading across arrays.

3.5 Real-World Applications

Outdoor characterization techniques must be able to accurately acquire data with minimal costs, little to no impedance on power production, and simplistic implementation to be effective. Implementation of these techniques may vary based on the system type and size, as small residential systems and large utility scale systems each present their own unique constraints.

In the United States, the average residential system size is between 4 kW to 7 kW [122]. These systems offer the advantage of having smaller string sizes, providing more resolution for Suns-V_{OC} measurements. The disadvantage is that residential systems do not typically have on site weather stations for measuring irradiance and temperature. Therefore, irradiance sensor(s) and temperature sensor(s) need to be installed in strategic locations around the system. Multiple sensors may be needed if systems are installed with different tilt angles, though POA irradiance may be calculated from a single sensor [123]. Regarding data acquisition (DAQ), many commercially available data logger solutions currently exist. These data loggers can be placed between the PV and inverter to log data

such as current, voltage, power, and peripheral weather sensors. These data loggers can acquire all the data needed to perform Suns-V_{OC} measurements before the inverter(s) reach their threshold voltage, as well as perform Suns-V_{MP} measurements after the inverter(s) have turned on. This configuration may not be adequate if the inverter threshold voltage is too low, resulting in irradiance levels too low for Suns-V_{OC} measurements. A simple DC controlled relay can be used to alleviate the issue caused by low inverter threshold voltages while an irradiance sensor can be used as the control for the relay, allowing the solar output to bypass to the inverter once the Suns-V_{OC} measurement has been conducted. For more advanced design, data loggers can be developed specifically for the purpose of conducting Suns-V_{OC} measurements on residential systems.

Utility scale systems offer more flexibility due to their larger system sizes and unique designs that may vary from powerplant to powerplant. An advantage for utility scale systems is that onsite weather stations are placed within the fielded modules. When designing an integrated outdoor Suns-V_{OC} system, one must consider the proximity of the weather stations to specific strings. If a weather station is placed too far from specific PV strings, irradiance and temperature data may not be an accurate representation for the respective strings. This can be problematic in instances of varying topography during low angle of incidences, such as sunrise and sunset, and during periods of partial shade from cloud coverage.

These powerplants may also deploy their own unique SCADA (Supervisory Control and Data Acquisition) systems to monitor and control their generation. Capturing Suns-V_{OC} data by use of the SCADA is unlikely because SCADA systems do not typically

capture open circuit voltage. However, SCADA systems may be used to capture Suns-V_{MP} data, without any new hardware.

Acquiring the open-circuit voltage measurements for Suns-V_{OC} is largely dependent upon the desired resolution. When string-level resolution is desired, DAQ hardware can be placed within the combiner boxes. There are currently several commercially available monitoring devices, primarily used to monitor string voltages and currents. By placing the hardware within a combiner box, one DAQ can be used to monitor several different strings at the same time.

For higher monitoring resolution, such as individual modules, a similar approach to that of module-level power electronics (MLPE) can be applied. DAQ hardware can be placed in parallel between individual modules, collecting open circuit voltages at desired ranges of irradiance. An irradiance sensor can be used as a controller for when data should be collected, subsequently placing the module back in series with the string. This method is benefitted by having localized irradiance measurements and more control precision, but it requires the use of an extra sensor. Contrasted to an irradiance sensor, the DAQ can simply be programmed to collect data by specific dates and times based on the respective sun positions. Using the date and time would not require an additional sensor, but it would need to be programmed individually based on the geographic coordinates. Finally, the module's open circuit voltage can be used for the DAQ shutoff threshold. This would be the simplest method to implement, yet it would provide a more inconsistent operation. Degraded modules may take longer to reach this threshold voltage, consequently impeding the power production of the respective string. The approach of applying DAQ to individual

modules can be used for both residential and utility installations, though utility installations may only sample a statistical representation of modules.

This work proves that Suns-V_{OC} can be applied outdoors on PV modules and arrays, providing much of the same useful diagnostic information as commonly found in indoor Suns-V_{OC}, including diode parameters free from the effects of series resistance. Collection of long-term PV performance data from light I-V curves is often impeded by logistical difficulties, variable weather, and the requirement to sweep I-V curves during major production hours of high, uniform irradiance. The results of this study prove that high-quality diagnostic parameters from Suns-V_{OC} can be performed during low irradiance conditions, perhaps even before the system voltage reaches the inverter startup threshold. Suns-V_{OC} parameters derived from periods of exclusively using low irradiance, compared to using the entire range of irradiance, yield consistent relative deltas of 0.5% in V_{OC} at 0.1 suns, 0.9% in pFF, and 0.4% in pP_{MP}. If the data collection methodology is consistent, exclusively using low irradiance periods is valuable for monitoring changes over time. Outdoor Suns-V_{OC} is also robust against partial shading, meaning that instances of interrow self-shading should have minimal impacts on the Suns-V_{OC} parameters. Measurements can be expected to be within 5% of true pP_{MP} in nearly all partial shading conditions. In the outdoor measurements, differences in performance metrics from daily and seasonal fluctuations produce maximum variations on the order ±1%. Applications may include but are not limited to reliability studies, impeding fault detection, and performance monitoring.

4 SUNS-VR

Suns-V_{OC} only captures data using the open-circuit voltage, excluding parameters related to current and power. A complete current-voltage (I-V) sweep is often conducted to complement Suns-V_{OC} to obtain parameters related to current and impacts of R_S. A simple adaptation to Suns-V_{OC}, termed Suns-Voltage-Resistor (Suns-VR), can be used to extract parameters related to power and efficiency. The technique involves placing a resistor across the device when conducting Suns-V_{OC} measurements. The Suns-VR measurement complements, rather than replaces the Suns-V_{OC} technique, and the combination of the two provides a more comprehensive characterization of solar cell loss mechanisms [124].

4.1 Principal of Suns-VR

Conceptually, the output power of a photovoltaic module is measured by placing a variable resistor across the module and measuring corresponding current-voltage points as the resistor is varied under uniform illumination. This concept is commonly performed using an electronic variable resistor [125] but can be performed manually with a variable resistor [126]. Figure 4.1 shows an example of how the power is calculated using the variable resistor technique, where the numbers are respective resistor values. It may be challenging when manually sweeping to hit the exact maximum power point (M_{PP}) with a constant cell temperature and illumination, due to the resolution of the variable resistor.

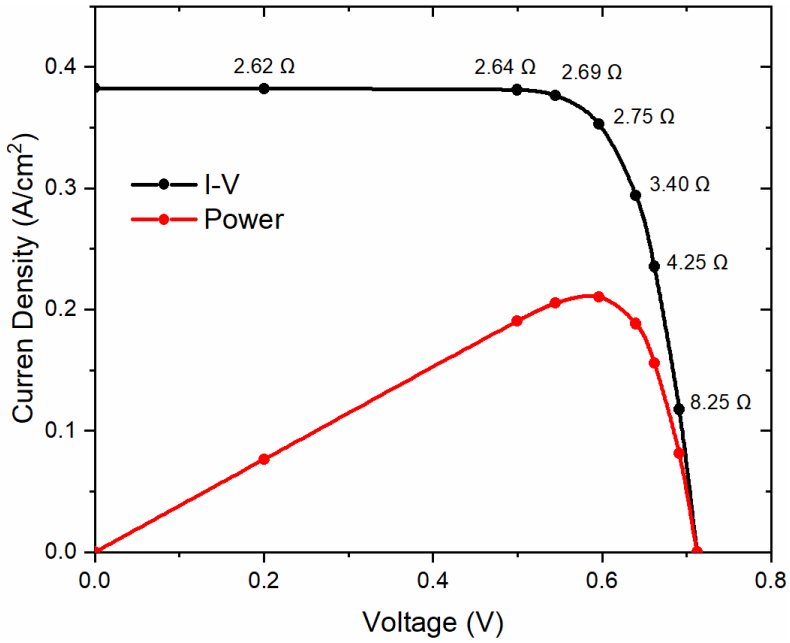

Figure 4.1. A Simulated Manual Measured I-V and P-V with a Variable Resistor. Individual Points Are Labeled with the Resistor Value Used to Measure the Respective Voltage and Current.

The Suns-VR procedure for measuring the module output power is shown in figure 2. A resistor is placed across the module's output and measured while varying the light intensity. The load resistance (R_{Load}) can be estimated using:

$$R_{Load} = \frac{V_{MP}}{I_{MP}} \approx \frac{V_{oc}}{I_{sc}} \tag{24}$$

where V_{MP} is the voltage at the maximum power point and I_{MP} is the current at the maximum power point. If the resistance value is not optimal, then the efficiency reported at the curve maximum is still the maximum power point, just at a light intensity different from one sun. A more optimal resistor value may provide a better approximation of diode parameters under one-sun illumination.

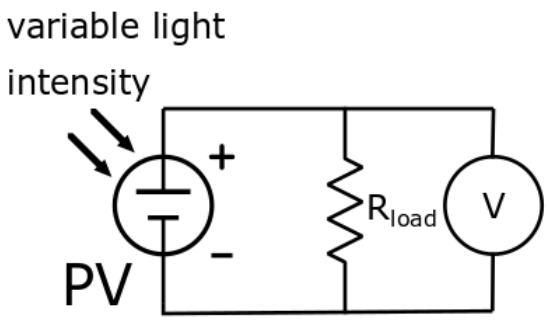

Figure 4.2 A Circuit Schematic Displaying How to Retrofit Suns-V_{OC} for Suns-VR Measurements.

Using Suns-VR, the power output is calculated using:

$$Power = \frac{{V_{load}}^2}{Suns \times R_{load}} \tag{25}$$

where the load resistance is a stable known value, V_{Load} is the measured voltage, and Suns is the measured incident irradiance. If drift within the load resistor is suspected, e.g. due to heating, the current should be measured separately.

4.1.1 Implementation of Suns-VR

The illumination source must be varied from 0 to 3 suns, depending on the size of the load resistor. A slightly oversized load resistor requires a maximum of less than 1 sun, whereas an undersized load resistor may need up to 3 suns. The light variation can either be done with an electronic flash, neutral density filters, or simply angling the module to the light source such as the sun. Uniformity across the module is key to mitigating mismatch error. An indoor environment must be clear of objects that may cause reflections and scattered light. The setup must be optimized to ensure appropriate light intensity distributed at a uniformity appropriate for the module size.

Implementing Suns-VR in an outdoor environment is possible, but more variables are introduced as compared to an indoor measurement. One must ensure uniform light is available, by measuring during clear sky conditions. If the module is being tilted to manually vary the light, reflections must be considered [127], [128]. The module could be measured throughout the course of a day to achieve natural light variations, but a large power resistor must be used to mitigate the effects of drift due to temperature extremes from power dissipation. The module operating temperature is arguably the most important variable impacting outdoor measurements. Module voltages proportionately decrease with increased temperatures [100]. Measurements are likely to be recorded at different temperatures, therefore requiring temperature normalization.

4.1.2 Simulation of Suns-VR

The data from the Suns-VR can be plotted in a variety of ways. By plotting the data normalized to irradiance, the apex of the curve is equivalent to the M_{PP}. Figure 4.3 displays the modeled normalized power output using different load resistances. When the load resistor is inadequately sized, the M_{PP} is reported at a light intensity different to one sun. However, efficiency changes slowly with light intensity so the value of M_{PP} at the apex is close to the one-sun value even for resistance values with a large departure from the ideal (15 Ω in this case).

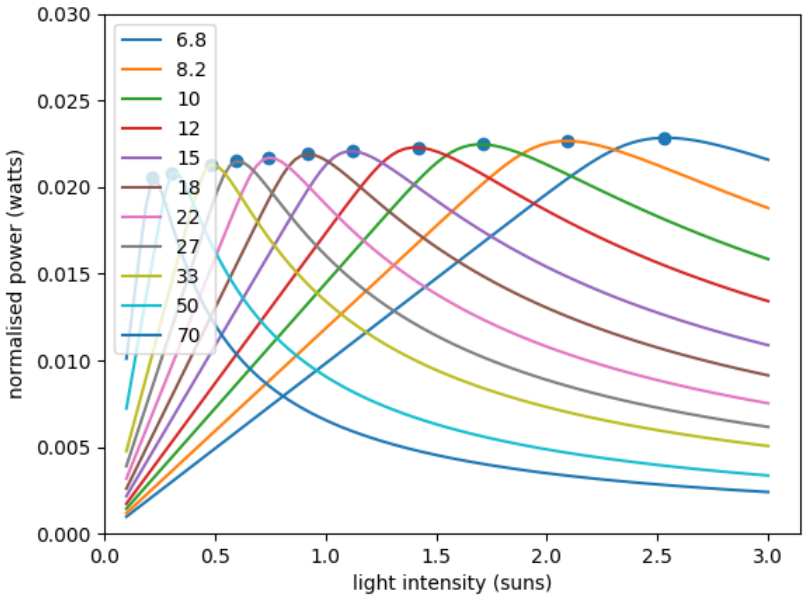

Figure 4.3. Modeled Normalized Power of a Solar Module Using Suns-VR Methodology with Varying Resistor Values as Denoted in the Legend.

4.2 Indoor Suns-VR Measurements

An 8-cell monocrystalline silicon module was fabricated for indoor measurements using Suns-VR. The 8-cell module is comprised of a single cell diced into eight equal pieces and soldered together in a series connection. Therefore, the power of the module remains unchanged, but the higher voltages allow for usage of more common resistor values. A monocrystalline silicon cell with similar encapsulation of glass-EVA-backsheet was used as the sensor cell.

4.2.1 Irradiance Measurements

Measurements were conducted at approximately 25 °C using a Xenon flash as the illumination source. Using a horizontal orientation, the flash was setup at a height of 1.5 m and a lateral distance of 3 m from the module surface. A 45x60 cm rectangular flash

diffuser was used to disperse light equally across the surface area of the module. Figure 4.4 shows the spatial uniformity of light across the 1 x 1.5 m surface in units of normalized suns.

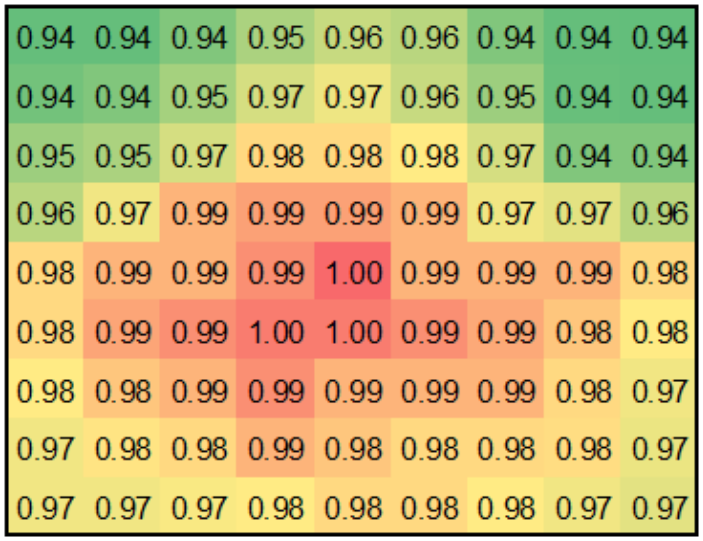

Figure 4.4. Spatial Uniformity of a Xenon Flash Located 3 m from the Module Surface in the Units of Normalized Suns.

The uniformity in Figure 4.4 has a deviation of roughly 5% from the center to the outside corners. It results in an error of similar magnitude when measuring modules greater than 1 m in length due to cell mismatch. Because the module in this experiment is less than 0.2 m in length, the flash mismatch is less than 2%.

4.2.2 Single Module Validation Testing

Using the module's ratings of 1.19 A for I_{MP} and 3.86 V for V_{MP}, a resistor of roughly 3.2 Ω was needed to induce operation at M_{PP} at approximately one sun. Resistor values of 2.2 Ω, 3.3 Ω, 3.9 Ω, 4.7 Ω, 5.6 Ω, and 6.8 Ω were used to quantify the resulting differences. The measured raw results per respective flash are displayed in Figure 4.5.

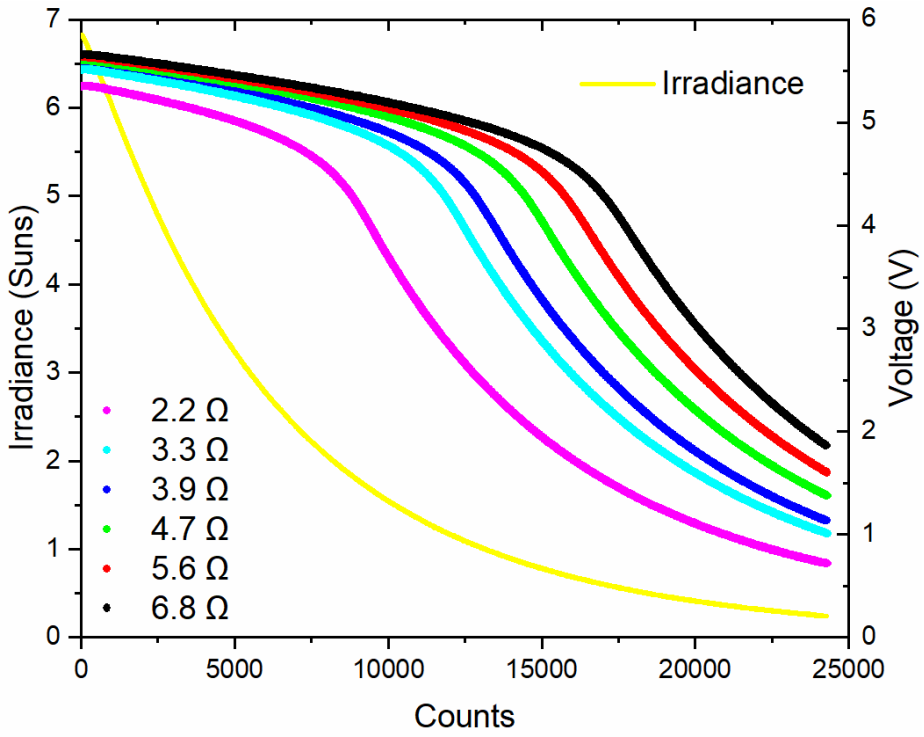

Figure 4.5 Raw Data from Suns-VR Measurements Using Various Resistor Values.

The raw data graphed in Figure 4.5 uses "counts" for the x-axis, though the entire measurement took approximately one second. For smaller resistor values, the apex of the curve is reached earlier at higher light intensities. The normalized powers are plotted below in Figure 4.6. The apex of each curve is the maximum power (P_{MAX}) for each resistor value.

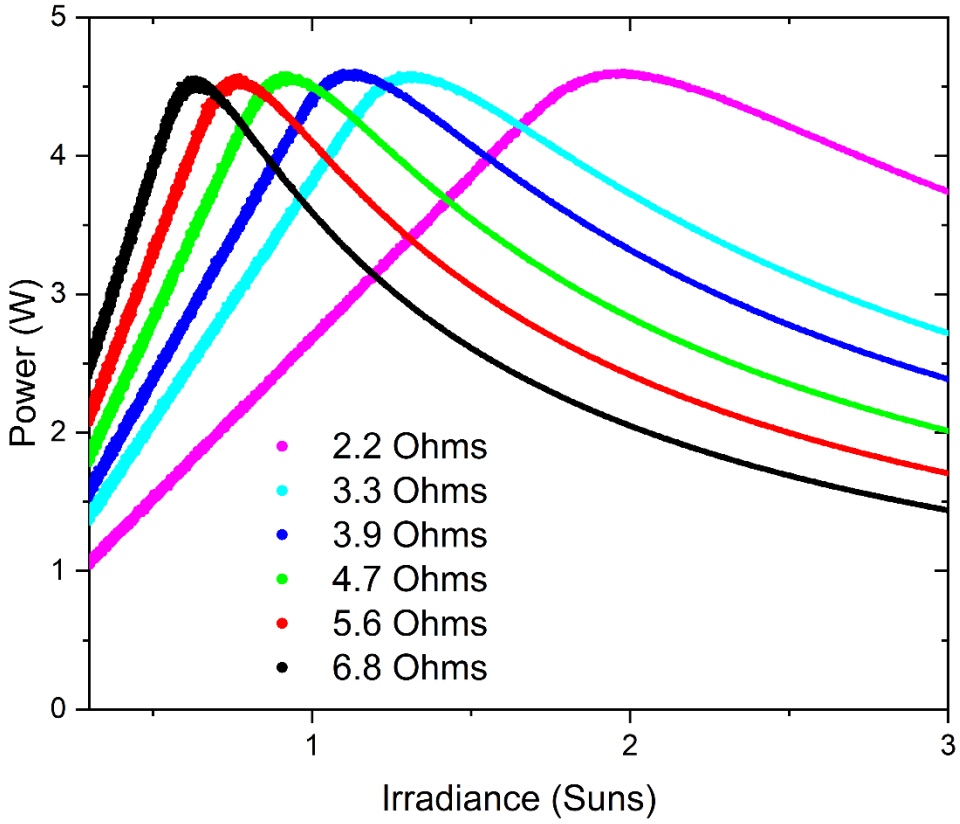

Figure 4.6. Power as a Function of Light Intensity Using Suns-VR with Different Resistor Values on a Crystalline Silicon Module.

Current related parameters can be derived by further analyzing Figure 4.6. The slope of the curve leading up to the M_{PP} provides the I_{SC} as:

$$I_{SC} = \frac{\Delta Voltage}{\Delta Suns \times R_{load}} \tag{26}$$

where $\Delta Voltage$ is the change in voltage (y axis) and $\Delta Suns$ is the change in irradiance (x axis). It is important to only use the linear portion of the slope before reaching the M_{PP}. Table 4.1 provides the P_{MAX} and the sun intensity at which the M_{PP} was attained, the I_{SC} as calculated from (26), the efficiency as calculated by Suns-VR, and the corresponding values when using a conventional flash tester to measure the I-V curve.

Table 4.1. Suns-VR Parameters Using Various Resistor Sizes Compared to I-V Measurements on a Silicon Module.

Resistor Value (Ω)	P_{MAX} (W)	Suns at P_{MAX}	I_{SC} (A)	n
2.2	4.61	1.98	1.11	20.49%
3.3	4.59	1.27	1.09	20.42%
3.9	4.61	1.1	1.09	20.49%
4.7	4.59	0.9	1.08	20.40%
5.6	4.58	0.77	1.08	20.34%
6.8	4.56	0.63	1.08	20.27%
I-V Flash	4.60	1	1.24	20.42%

As seen in the results, increased resistor sizes decrease the level of illumination needed to measure the M_{PP}. The decreased level of illumination yields a slightly lower value for both P_{MAX} and efficiency. The most notable difference is the values of ISC from Suns-VR measurements as compared to the I-V flash method. This discrepancy may be due to spectral differences from using two different flash sources. Another possible explanation is the distance from the illumination source for both measurements. Suns-VR measurements were conducted approximately 3 m from the flash source, while I-V testing was conducted approximately 0.75 m from the flash source. I-V measurements may have yielded higher current measurements from enhanced reflection off the backsheet, while the increased distance from Suns-VR measurements may not have the additional reflection from the white backsheet.

By using different size load resistors, the M_{PP} reported were all within a deviation of roughly 1.5%. This deviation falls within the resistor's tolerance of ± 5%. This suggests that the results are still valid if the resistor is not sized exact to the optimal size.Varying the load resistor size can purposely done to induce different injection levels without manipulating the illumination source. By oversizing the load resistor, the M_{PP} is found at a

lower injection level, and vice versa. Intentionally manipulating the injection level can induce different recombination effects. Auger recombination typically manifest at high injection levels [129]. Analyzing Suns-VR at low injection level provides more specific insight to how Shockley-Read-Hall (SRH) recombination effects are potentially impacting the module [130].

Further optimization of the diffusers to improve uniformity enables the testing modules of larger surface areas. This work was conducted to provide practicality at a smaller scale but can easily be scaled up with a proper illumination source. Suns-VR is a simple method to enhance the commonly used Suns-V_{OC} characterization technique. Any Suns-V_{OC} assessment can be easily retrofitted to perform Suns-VR with the addition of a properly sized load resistor. Suns-VR provides analysis of the M_{PP}, efficiency, and I_{SC} at different illumination levels. Suns-VR measurements agreed with flash testing I-V measurements, with less than 1% difference for P_{MAX}, 1% difference for efficiency, and 8% difference for I_{SC}.

5 APPLICATIONS OF OUTDOOR CHARACTERIZATION

There is a multitude of PV systems with different sizes, configurations, installation types (e.g., residential or utility-size), using distinctive cell and module architectures. As result, there is not a universal solution to measure and characterize those systems. Furthermore, depending on the system owner objectives, applications may include instant performance monitoring, automatic fault detection, long term degradation analysis, warranty claims, just to name a few. This section discusses how outdoor characterization can be used for various applications.

In the literature, the testing practices are normally divided into two groups “off-line” and “in-situ” testing. In the off-line testing, the PV module/array is typically disconnected from the system when measured. The off-line testing can be either performed on-site or in an indoor location off-site [131], [132]. The transportation of modules to off-site locations can induce defects, such microcracking, leading to misleading conclusions. Alternatively, the PV Mobile Lab trailer system provides on-site (although still off-line) light I-V and Suns-V_{OC} measurements [133]. Since the off-line testing normally requires a considerable amount of manual labor, it is costly, with very limited scalability, and not suitable to deliver instant performance monitoring or automatic fault detection. On the other hand, this type of testing provides high-quality and quantitative analyses of the module performances, which can be used for long-term degradation analysis [134] and warranty claims [135]. More recently, electrostatic voltmeters have been used as a non-contact approach to measure the I-V characteristics of modules without the need of disconnecting strings, easing these type of measurements [136].

In-situ testing uses dedicated hardware to measure the PV systems continuously. The characterization techniques range in use, such as high granular resolution via module-level I-V tracers, to analysis involving the entire power output as a whole. Module-level in-situ I-V testers have been used for system monitoring [137], degradation analysis [98], and real-time fault detection [138]. Techniques have also been established for in-situ measurements at the array level, which have been used for automatic fault detection [139]. The rise of wireless sensors have enabled these measurements to be conducted in a more scalable way, as compared to wired sensors [140]. The in-situ measurement techniques are typically performed on a smaller statistical sample of the PV plant, due to the cost of needing permanent hardware. There are opportunities for integrating the data acquisition hardware into system components such as DC optimizers and inverters [141]. Also, in-situ I-V scans have little to no impact on power production, as scans are typically completed in less than two seconds. The use of in-situ measurements has increased with the exponential increase of installed PV modules, resulting in large quantities of data. Different machine learning approaches have been implemented to analyze this data. One particular method was developed to extract I-V features and create subsequent Suns-V_{OC} plots, by using STC translated I_{SC}-V_{OC} data [112], [142]. This methodology was proven to be robust to steps, caused by cell mismatch and shading, in the I-V data. It was used as long-term degradation analysis by calculating year-to-year performance loss rates of different commercial modules located in different climate zones, analyzing over 3 million I-V curves [143]. This methodology benefits from gathering detailed diode parameters, which can be used to calculate uniform current losses, recombination losses, R_S losses, and current mismatch losses. Further research is necessary to understand if such methodology can be applied to

systems larger than a single module. Using this approach, Figure 5.1 shows the power loss mechanisms calculated in each step, starting from the initial pseudo I-V curve and ending at the actual measured I-V curve from a PV module [142]. Other approaches have been used to gather real-time data, without needing full in-situ I-V measurements. For example, NREL developed an approach that capitalized on Suns-V_{OC} principles to measure real-time series resistance [144].

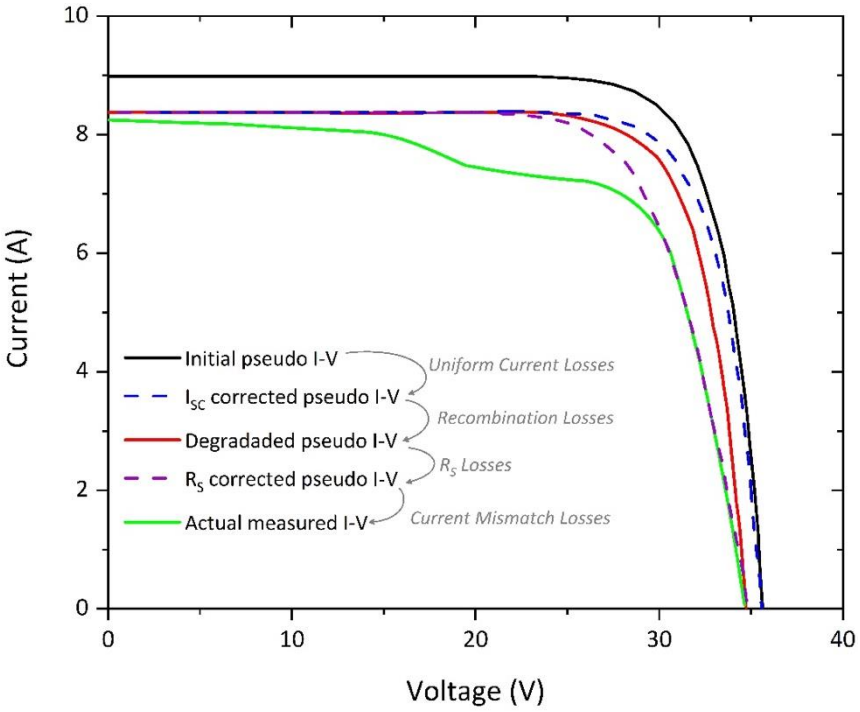

Figure 5.1. Power Loss Calculation From In-Situ Pseudo I-V Analysis via [142].

The data collected from I-V curves, whether conducted in-situ or during an off-line evaluation, provides highly quantitative metrics regarding performance and respective losses. An attractive alternative to I-V tracing is to measure the maximum voltage, current, and power of the PV system. This method is widely used within industry for Supervisory

Control and Data Acquisition (SCADA) systems for real-time monitoring, because of the simple integration with inverter data collection. The maximum-power point data can provide a quick qualitative snapshot for any catastrophic issues impacting the power production. Different analyses of this maximum-power point data have been used for degradation evaluation: (1) ratio of maximum power to plane of array irradiance [145]; (2) the fraction of maximum power to nameplate rating, termed performance ratio [146]; (3) Photovoltaics for Utility Scale Applications (PVUSA) which involves a translation of maximum power based on a set of standardized test conditions for irradiance, temperature, and wind speed [147]. These analyses fail to offer detailed information regarding the specific degradation mechanisms as compared to in-situ I-V curves [148]. The Suns-V_{MP} capitalizes on the methodology of Suns-V_{OC}, but instead of measuring the V_{OC}, measures the V_{MP}, which includes the effects of series resistance [149]. Once the data has been collected and preprocessed, an I-V fitting algorithm is used to extract diode parameters which can be used for degradation analysis. The methodology relies on knowing initial module parameters, having a measurement window of at least two to three days, and assuming a maximum degradation rate of 1% per day is not exceeded. Further work is necessary to better understand intra-string variability regarding string-level measurements.

The needs of each specific PV system and owner should define which characterization method is better suited. Some applications, such as performing quantitative degradation analysis, may require more costly but more comprehensive characterization techniques. In other cases, low-cost characterization techniques may be sufficient to validate qualitatively the system performance. In other words, there is no “one size fits all” solution for monitoring PV systems. As the systems continue to increase in

size and complexity, better strategies to collect and analyze data will be required to facilitate early detection of faults or degradation issues that can lead to revenue loss and warranty forfeit.

6 CONCLUSION

Photovoltaic systems were once only viable for utility or rooftop installations. Fueled by the decarbonization efforts, PV is now being considered to integrate with almost anything. New fields of research have developed such as combining agriculture with PV (agriPV) [150], combining aquaculture with PV (aquaPV) [151], using PV for transportation [152], integrating PV into building materials (BIPV) [153], floating PV [154], etc. The rise of these industries means characterization and system monitoring needs to be prioritized to ensure successful implementation. The diverse nature of the different PV systems requires a diverse approach for monitoring.

This work has examined the accuracy of temperature-translated outdoor Suns-V_{OC} compared to indoor measurements. For best accuracy, module temperature should be measured meeting requirements outlined by IEC 61583, and an appropriate cell temperature model should be applied. On-site weather station data, comprised of POA irradiance, ambient temperature, and wind speed has proved to be an effective alternative to measuring the backsheet temperature and irradiance of each module; pP_{MP} results are within ±1% of the respective backsheet temperature results. With appropriate temperature translation, the parameters provided by Suns-V_{OC} curves taken in an outdoor setting may provide reliable degradation quantification and attribution without interfering with normal system operation.

The use of outdoor Suns-V_{OC} has proven to yield accuracies within 1% of indoor Suns-V_{OC} measurements. This at first may not seem useful in detecting degradation, but repeatability is more vital than accuracy. This work provided daily variations of less than

+/- 0.5% in pseudo parameters. This means that outdoor Suns-V_{OC} can potentially be used to analyze for degradation changes on the magnitude of more than 0.5% when comparing over daily variations. This may be useful in detecting major degradation mechanisms such as potential induced degradation (PID), which would result in more extreme daily variations. Outdoor Suns-V_{OC} can potentially increase power output and system lifespan if reversable degradation mechanisms are seen early.

Outdoor Suns-V_{OC} does suffer from various data collection obstacles that could be addressed in future work, as laid out in Chapter 7. The translated Suns-V_{OC} results are extremely sensitive to temperature. The methods proposed in this work assume constant temperature across the surface of the module. In instances of major temperature variations, the methodology may not prove sufficient. The extreme sensitivity also means that many of the extractable variables may not be used for proper degradation analysis. For example, ideality factors may often be inaccurate due to both the temperature sensitivity and the poor resolution at low light intensities. Some of these challenges may be alleviated with higher accuracy sensors, but at a higher cost monitoring system.

The outdoor characterization industry was addressing a real challenge of how to capture data when the work for this dissertation was first started. The golden standard of I-V curve tracing proved to be difficult for several reasons mentioned within this thesis. This work was conducted to address some of these challenges by developing an alternative to I-V curve tracing. At the finality of this dissertation, I-V curve tracing has become more viable. Many inverters have started using integrated I-V testers, which have started providing the industry with a more practical method to acquiring quantifiable outdoor

characterization data. This does not mean outdoor Suns-V_{OC} is obsolete, but it does potentially limit the effectiveness when compared to I-V testing. Nonetheless, outdoor Suns-V_{OC} may serve as a potential option for addressing outdoor characterization of PV modules and systems.

7 FUTURE WORK

The findings in this dissertation provide the opportunity for future research to be performed. This section has been written to include both suggestions on how this specific work can be expanded and where efforts for future work should be focused to address the needs of the photovoltaic industry.

Outdoor Suns-V_{OC} would benefit from increased accuracy which may be possible by investigating several different factors. This work only analyzed data collection with resolution of 1 minute. Further experimentation should be conducted to better understand if higher resolution data enhances accuracy. This may be constrained due to the ability to collect data in large-scale applications, but it should be better understood. This opportunity could also be used to address the minimal amount of data that needs to be collected for a proper analysis. This work analyzed the data collected only during a single day of low irradiance data. The daily and seasonal variations may benefit from a wider range of data collection before analysis can be performed. This would potentially allow for more temperature variation in the irradiance voltage pairs.

Improvements to accuracy may also be possible when using a weather station for environmental data acquisition. This work used empirically determined coefficients from another study to justify how the wind would impact the system's maximum temperature and rate of cooling. The sensitivity analysis performed for these coefficients proved that minor changes could heavily influence the translated results. Therefore, future work should be performed to experimentally determine these coefficients and examine the impacts on the accuracy of translated results.

Another opportunity related to weather stations is to better understand the relationship of the weather station's proximity to the respective test system. This work was performed with a weather station that was located less than 10 m away from the PV system. In real world conditions, weather stations can be located much further away from the PV system. The larger distances may have a negative impact on accuracy as ambient temperature and wind speed may be different at the test location versus what is measured at the weather station. The impact of this distance and the influence of translated Suns-V_{OC} parameters should be further investigated in future work.

Multiple future work opportunities for improvement of outdoor Suns-V_{OC} have been discussed. Using the potential findings from this future work, Suns-V_{OC} could be used for an outdoor degradation study. This study would potentially address the viability for real world applications and give insight to degradation mechanisms detectable by Suns-V_{OC}. This study would ultimately be a compilation of this work and all the suggested future work.

The PV industry is finally at a point where outdoor data collection is more practical and is starting to be implemented. The resulting opportunity that surfaces is how to analyze this data. In my opinion, effort should be focused on developing machine learning approaches to better use this data, driven by applications such as degradation analysis and fault detection. These machine learning algorithms can be used to increase overall revenue from PV systems, increase system lifespans, etc. This future work suggestion is quite broad because there are almost endless applications for what to do with this data. As the industry

starts implementing these applications, there will be a larger push to implement outdoor characterization.

REFERENCES

[1] G. Masson and I. Kaizuka, “Trends in Photovoltaic Applications,” 2021.

[2] G. M. Wilson *et al.*, “The 2020 photovoltaic technologies roadmap,” *J. Phys. D. Appl. Phys.*, vol. 53, no. 49, p. 493001, Sep. 2020.

[3] R. Bhoopathy, O. Kunz, R. W. Dumbrell, T. Trupke, and Z. Hameiri, “Outdoor Implied Current–Voltage Measurements of an Individual Encapsulated Cell in a Module,” *IEEE J. Photovoltaics*, vol. 11, no. 1, pp. 164–173, Jan. 2021.

[4] M. Owen-Bellini *et al.*, “Advancing reliability assessments of photovoltaic modules and materials using combined-accelerated stress testing,” *Prog. Photovoltaics Res. Appl.*, vol. 29, no. 1, pp. 64–82, 2021.

[5] “IEC 61215-1:2021 - Terrestrial photovoltaic (PV) modules - Design qualification and type approval - Part 1: Test requirements,” Geneva, 2021.

[6] S. Kurtz *et al.*, “A framework for a comparative accelerated testing standard for PV modules,” in *2013 IEEE 39th Photovoltaic Specialists Conference (PVSC)*, 2013, pp. 132–138.

[7] M. Owen-Bellini *et al.*, “Combined-Accelerated Stress Testing for Advanced Reliability Assessment of Photovoltaic Modules,” 2020.

[8] S. Spataru, P. Hacke, and M. Owen-Bellini, “Combined-Accelerated Stress Testing System for Photovoltaic Modules,” in *2018 IEEE 7th World Conference on Photovoltaic Energy Conversion (WCPEC) (A Joint Conference of 45th IEEE PVSC, 28th PVSEC 34th EU PVSEC)*, 2018, pp. 3943–3948.

[9] P. Sánchez-Friera, M. Piliougine, J. Peláez, J. Carretero, and M. de Cardona, “Analysis of degradation mechanisms of crystalline silicon PV modules after 12 years of operation in Southern Europe,” *Prog. Photovoltaics Res. Appl.*, vol. 19, no. 6, pp. 658–666, 2011.

[10] B. Kroposki, R. Margolis, and D. Ton, “Harnessing the sun,” *IEEE Power Energy Mag.*, vol. 7, no. 3, pp. 22–33, 2009.

[11] P. Rappaport, “The photovoltaic effect and its utilization,” *Sol. Energy*, vol. 3, no. 4, pp. 8–18, 1959.

[12] A. Augusto, A. Killam, H. Wilterdink, and S. Bowden, “Measuring Outdoor I-V Characteristics of PV Modules and Systems,” *unpublished*.

[13] P. Würfel, “Semiconductors,” in *Physics of solar cells: from basic principles to advanced concepts*, 2nd, updat ed., Wiley-VCH, 2009, pp. 71–74.

[14] R. Pierret, “PN Junction Diode: I-V Characteristics,” in *Semiconductor Device Fundamentals*, Addison-Wesley, Ed. 1995, pp. 235–259.

[15] O. Breitenstein, J. Bauer, and J. P. Rakotoniaina, “Material-induced shunts in multicrystalline silicon solar cells,” *Semiconductors*, vol. 41, no. 4, pp. 440–443, 2007.

[16] “Solar cells—Operating principles, technology and system applications: Martin A. Green, Prentice Hall, 1982, 256pp: Cost $27.95. New Jersey,” *Sol. Energy*, vol. 28, no. 5, p. 447, 1982.

[17] M. Wolf and H. Rauschenbach, “Series resistance effects on solar cell measurements,” *Adv. Energy Convers.*, vol. 3, no. 2, pp. 455–479, 1963.

[18] “BiHiKu - Canadian Solar Datasheet.” [Online]. Available: https://static.csisolar.com/wp-content/uploads/2019/12/21140025/CS-Datasheet-BiHiKu_CS3W-MB-AG_v5.8_EN.pdf.

[19] T. Barnes *et al.*, “DuraMAT : Accelerating Improvements in Module Durability,” 2019.

[20] J. A. Tsanakas, L. Ha, and C. Buerhop, “Faults and infrared thermographic diagnosis in operating c-Si photovoltaic modules: A review of research and future challenges,” *Renew. Sustain. Energy Rev.*, vol. 62, pp. 695–709, 2016.

[21] A. Morlier, M. Siebert, I. Kunze, G. Mathiak, and M. Köntges, “Detecting Photovoltaic Module Failures in the Field During Daytime With Ultraviolet Fluorescence Module Inspection,” *IEEE J. Photovoltaics*, vol. 7, no. 6, pp. 1710–1716, Nov. 2017.

[22] J. D. Berghold, P. Clemens, A. Fladung, C. Sobottka, T. Weber, and S. Koch, “Outdoor Electroluminescence Imaging of Crystalline Photovoltaic Modules: Comparative Study between Manual Ground-Level Inspections and Drone-Based Aerial Surveys,” 2016.

[23] R. Bhoopathy, O. Kunz, M. Juhl, T. Trupke, and Z. Hameiri, “Outdoor photoluminescence imaging of solar panels by contactless switching: Technical considerations and applications,” *Prog. Photovoltaics Res. Appl.*, vol. 28, no. 3, pp. 217–228, 2020.

[24] G. B. Alers, J. Zhou, C. Deline, P. Hacke, and S. R. Kurtz, “Degradation of individual cells in a module measured with differential IV analysis,” *Prog. Photovoltaics Res. Appl.*, vol. 19, no. 8, pp. 977–982, 2011.

[25] J. Karas *et al.*, “Degradation of copper-plated silicon solar cells with damp heat stress,” *Prog. Photovoltaics Res. Appl.*, vol. 28, no. 11, pp. 1175–1186, 2020.

[26] J. Karas *et al.*, “Damp Heat Induced Degradation of Silicon Heterojunction Solar Cells With Cu-Plated Contacts,” *IEEE J. Photovoltaics*, vol. 10, no. 1, pp. 153–158, Jan. 2020.

[27] “IEC TS 61836:2016 - Solar photovoltaic energy systems - Terms, definitions and symbols,” Geneva, 2016.

[28] P. K. Dash, N. C. Gupta, R. Rawat, and P. C. Pant, “A novel climate classification criterion based on the performance of solar photovoltaic technologies,” *Sol. Energy*, vol. 144, pp. 392–398, 2017.

[29] M. E. Meral and F. Dinçer, “A review of the factors affecting operation and efficiency of photovoltaic based electricity generation systems,” *Renew. Sustain. Energy Rev.*, vol. 15, no. 5, pp. 2176–2184, 2011.

[30] R. Eke, T. R. Betts, and G. R., “Spectral irradiance effects on the outdoor performance of photovoltaic modules,” *Renew. Sustain. Energy Rev.*, vol. 69, pp. 429–434, 2017.

[31] D. L. King, J. A. Kratochvil, and W. E. Boyson, “Measuring solar spectral and angle-of-incidence effects on photovoltaic modules and solar irradiance sensors,” in *Conference Record of the Twenty Sixth IEEE Photovoltaic Specialists Conference - 1997*, 1997, pp. 1113–1116.

[32] K. V. S. Badarinath, S. K. Kharol, D. G. Kaskaoutis, and H. D. Kambezidis, “Influence of atmospheric aerosols on solar spectral irradiance in an urban area,” *J. Atmos. Solar-Terrestrial Phys.*, vol. 69, no. 4, pp. 589–599, 2007.

[33] Á. Fernández-Solas, L. Micheli, F. Almonacid, and E. F. Fernández, “Optical degradation impact on the spectral performance of photovoltaic technology,” *Renew. Sustain. Energy Rev.*, vol. 141, p. 110782, 2021.

[34] G. Nofuentes, B. García-Domingo, J. V Muñoz, and F. Chenlo, “Analysis of the dependence of the spectral factor of some PV technologies on the solar spectrum distribution,” *Appl. Energy*, vol. 113, pp. 302–309, 2014.

[35] A. Virtuani, H. Müllejans, and E. D. Dunlop, “Comparison of indoor and outdoor performance measurements of recent commercially available solar modules,” *Prog. Photovoltaics Res. Appl.*, vol. 19, no. 1, pp. 11–20, 2011.

[36] T. Minemoto *et al.*, “Effect of spectral irradiance distribution on the outdoor performance of amorphous Si//thin-film crystalline Si stacked photovoltaic modules,” *Sol. Energy Mater. Sol. Cells*, vol. 91, no. 2, pp. 120–122, 2007.

[37] M. R. Maghami, H. Hizam, C. Gomes, M. A. Radzi, M. I. Rezadad, and S. Hajighorbani, “Power loss due to soiling on solar panel: A review,” *Renew. Sustain. Energy Rev.*, vol. 59, pp. 1307–1316, 2016.

[38] A. Shaju and R. Chacko, “Soiling of photovoltaic modules- Review,” *{IOP} Conf. Ser. Mater. Sci. Eng.*, vol. 396, p. 12050, Aug. 2018.

[39] X. Li, D. L. Mauzerall, and M. H. Bergin, “Global reduction of solar power generation efficiency due to aerosols and panel soiling,” *Nat. Sustain.*, vol. 3, no. 9, pp. 720–727, 2020.

[40] C. Schill, S. Brachmann, and M. Koehl, “Impact of soiling on IV-curves and efficiency of PV-modules,” *Sol. Energy*, vol. 112, pp. 259–262, 2015.

[41] H. Kawamura *et al.*, “Simulation of I–V characteristics of a PV module with shaded PV cells,” *Sol. Energy Mater. Sol. Cells*, vol. 75, no. 3, pp. 613–621, 2003.

[42] M. C. Alonso-García, J. M. Ruiz, and F. Chenlo, “Experimental study of mismatch and shading effects in the I-V characteristic of a photovoltaic module,” 2005.

[43] R. K. Pachauri *et al.*, “Impact of Partial Shading on Various PV Array Configurations and Different Modeling Approaches: A Comprehensive Review,” *IEEE Access*, vol. 8, pp. 181375–181403, 2020.

[44] J. K. Kaldellis, M. Kapsali, and K. A. Kavadias, “Temperature and wind speed impact on the efficiency of PV installations. Experience obtained from outdoor measurements in Greece,” *Renew. Energy*, vol. 66, pp. 612–624, 2014.

[45] A. Srinivasa, R. King, S. Bowden, and A. Augusto, “Effect of Substrate Resistivity, Defects and Temperature on Silicon Heterojunction Solar Cells Performance,” in *2020 47th IEEE Photovoltaic Specialists Conference (PVSC)*, 2020, pp. 2171–2174.

[46] E. Skoplaki and J. A. Palyvos, “Operating temperature of photovoltaic modules: A survey of pertinent correlations,” *Renew. Energy*, vol. 34, no. 1, pp. 23–29, 2009.

[47] E. Skoplaki and J. A. Palyvos, “On the temperature dependence of photovoltaic module electrical performance: A review of efficiency/power correlations,” *Sol. Energy*, vol. 83, no. 5, pp. 614–624, 2009.

[48] S. Dubey, J. N. Sarvaiya, and B. Seshadri, “Temperature Dependent Photovoltaic (PV) Efficiency and Its Effect on PV Production in the World – A Review,” *Energy Procedia*, vol. 33, pp. 311–321, 2013.

[49] “IEC 62446-1:2016+AMD1:2018 CSV Consolidated version - Photovoltaic (PV) systems - Requirements for testing, documentation and maintenance - Part 1: Grid connected systems - Documentation, commissioning tests and inspection,” Geneva, 2018.

[50] B. Li, A. Migan-Dubois, C. Delpha, and D. Diallo, “Evaluation and improvement of IEC 60891 correction methods for I-V curves of defective photovoltaic panels,”

Sol. Energy, vol. 216, pp. 225–237, 2021.

[51] "IEC 60891:2021 - Photovoltaic devices - Procedures for temperature and irradiance corrections to measured I-V characteristics," Geneva, 2021.

[52] D. L. King, J. A. Kratochvil, and W. E. Boyson, "Photovoltaic Array Performance Model," 2004.

[53] J. Sandstrom, "A method for predicting solar cell current- voltage curve characteristics as a function of incident solar intensity and cell temperature," 1967.

[54] Y. Tsuno, Y. Hishikawa, and K. Kurokawa, "Temperature and Irradiance Dependence of the I-V Curves of Various Kinds of Solar Cells," *15th Int. Photovolt. Sci. Eng. Conf.*, 2005.

[55] C. W. Hansen and C. E. Martin, "Photovoltaic System Modeling. Uncertainty and Sensitivity Analyses."

[56] K. Kawagoe, Y. Hishikawa, and N. Yamada, "Outdoor Direct STC Performance Measurement of PV Modules Based on a Sun-Shading Technique," *IEEE J. Photovoltaics*, vol. 7, no. 6, pp. 1725–1730, Nov. 2017.

[57] D. R. Myers, "Solar radiation modeling and measurements for renewable energy applications: data and model quality," *Energy*, vol. 30, no. 9, pp. 1517–1531, 2005.

[58] R. Rösemann, C. Lee, H.-P. Meijer, and J. van der Voort, *A Guide to Solar Radiation Measurement, from Sensor to Application*, 2nd ed. Gengenbach Messtechnik, 2011.

[59] J. P. Kerr, G. W. Thurtell, and C. B. Tanner, "An Integrating Pyranometer for Climatological Observer Stations and Mesoscale Networks," *J. Appl. Meteorol. Climatol.*, vol. 6, no. 4, pp. 688–694, 1967.

[60] D. L. King, W. E. Boyson, and B. R. Hansen, "Improved accuracy for low-cost solar irradiance sensors," 1997.

[61] B. Schulz, T. Glotzbach, C. Vodermayer, G. Wotruba, M. Mayer, and S. Grünsteidl, "Evaluation of Calibrated Solar Cells and Pyranometers Regarding the Effective Irradiance Detected by PV Modules," 2010, pp. 4797–4800.

[62] A. Driesse, W. Zaaiman, D. Riley, N. Taylor, and J. Stein, "Indoor and Outdoor Evaluation of Global Irradiance Sensors," 2015.

[63] A. Driesse and W. Zaaiman, "Characterization of Global Irradiance Sensors for use with PV Systems," 2015.

[64] G. Wotruba *et al.*, “One Year Round Robin Testing of Irradiation Sensors - Measurement Results and Analyses,” 2009.

[65] A. de Montgareuil, J.-L. Martin, F. Mezzasalma, and J. Merten, “Main results of the first intercomparison campaign of European irradiance sensors at INES Cadarache (2007),” 2007.

[66] F. Vignola, P. Josh, C. Chiu, M. Dooraghi, M. Sengupta, and F. Mavromatakis, “Comparison of Pyranometers and Reference Cells on Fixed and One-axis Tracking Surfaces,” 2017, pp. 1–10.

[67] J. López Lorente, X. Liu, and D. J. Morrow, “Worldwide evaluation and correction of irradiance measurements from personal weather stations under all-sky conditions,” *Sol. Energy*, vol. 207, pp. 925–936, 2020.

[68] S. Karki, H. Ziar, M. Korevaar, T. Bergmans, J. Mes, and O. Isabella, “Performance Evaluation of Silicon-Based Irradiance Sensors Versus Thermopile Pyranometer,” *IEEE J. Photovoltaics*, vol. 11, no. 1, pp. 144–149, 2021.

[69] J. Polo, W. G. Fernandez-Neira, and M. C. Alonso-García, “On the use of reference modules as irradiance sensor for monitoring and modelling rooftop PV systems,” *Renew. Energy*, vol. 106, pp. 186–191, 2017.

[70] M. Jankovec and M. Topic, “Intercomparison of Temperature Sensors for Outdoor Monitoring of Photovoltaic Modules,” *J. Sol. Energy Eng.*, vol. 135, p. 31012, 2012.

[71] S. Krauter and A. Preiss, “Comparison of module temperature measurement methods,” *Conf. Rec. IEEE Photovolt. Spec. Conf.*, pp. 333–338, 2009.

[72] J. Kurnik, M. Jankovec, K. Brecl, and M. Topic, “Outdoor testing of PV module temperature and performance under different mounting and operational conditions,” *Sol. Energy Mater. Sol. Cells - Sol. ENERG MATER Sol. CELLS*, vol. 95, pp. 373–376, 2011.

[73] K. Nishioka, K. Miyamura, Y. Ota, M. Akitomi, Y. Chiba, and A. Masuda, “Accurate measurement and estimation of solar cell temperature in photovoltaic module operating in real environmental conditions,” *Jpn. J. Appl. Phys.*, vol. 57, no. 8S3, p. 08RG08, Jul. 2018.

[74] U. Jovanović, I. Jovanović, and D. Mančić, “Overview of Temperature Sensors for Temperature Measurement of PV Modules,” in *2018 26th Telecommunications Forum (TELFOR)*, 2018, pp. 1–8.

[75] E. Duran, M. Piliougine, M. Sidrach-de-Cardona, J. Galan, and J. M. Andujar, “Different methods to obtain the I–V curve of PV modules: A review,” in *2008 33rd IEEE Photovoltaic Specialists Conference*, 2008, pp. 1–6.

[76] Y. Zhu and W. Xiao, “A comprehensive review of topologies for photovoltaic I–V curve tracer,” *Sol. Energy*, vol. 196, pp. 346–357, 2020.

[77] J. I. Morales-Aragonés, M. Dávila-Sacoto, L. González, V. Alonso-Gómez, S. Gallardo-Saavedra, and L. Hernández-Callejo, “A Review of I-V Tracers for Photovoltaic Modules: Topologies and Challenges,” *Electronics*, vol. 10, p. 1283, 2021.

[78] J. Sayyad and P. Nasikkar, “Design and Development of Low Cost, Portable, On-Field I-V Curve Tracer Based on Capacitor Loading for High Power Rated Solar Photovoltaic Modules,” *IEEE Access*, vol. 9, pp. 70715–70731, 2021.

[79] M. Köntges *et al.*, “Review of Failures of Photovoltaic Modules,” 2014.

[80] C. E. Packard, J. H. Wohlgemuth, and S. R. Kurtz, “Development of a Visual Inspection Data Collection Tool for Evaluation of Fielded PV Module Condition,” United States, 2012.

[81] A. Pozza and T. Sample, “Crystalline silicon PV module degradation after 20 years of field exposure studied by electrical tests, electroluminescence, and LBIC,” *Prog. Photovoltaics Res. Appl.*, vol. 24, no. 3, pp. 368–378, 2016.

[82] “IEC 61853-1:2011 - Photovoltaic (PV) module performance testing and energy rating - Part 1: Irradiance and temperature performance measurements and power rating,” Geneva.

[83] R. Eke and H. Demircan, “Performance analysis of a multi crystalline Si photovoltaic module under Mugla climatic conditions in Turkey,” *Energy Convers. Manag.*, vol. 65, pp. 580–586, 2013.

[84] J. Teubner *et al.*, “Comparison of Drone-based IR-imaging with Module Resolved Monitoring Power Data,” *Energy Procedia*, vol. 124, pp. 560–566, 2017.

[85] C. Buerhop, D. Schlegel, M. Niess, C. Vodermayer, R. Weißmann, and C. J. Brabec, “Reliability of IR-imaging of PV-plants under operating conditions,” *Sol. Energy Mater. Sol. Cells*, vol. 107, pp. 154–164, 2012.

[86] A. G. Aberle, S. R. Wenham, and M. A. Green, “A new method for accurate measurements of the lumped series resistance of solar cells,” in *Conference Record of the Twenty Third IEEE Photovoltaic Specialists Conference - 1993 (Cat. No.93CH3283-9)*, 1993, pp. 133–139.

[87] R. A. Sinton and A. Cuevas, “A Quasi-Steady-State open-circuit voltage method for solar cell characterization,” *Proc. 16th Eur. Photovolt. Spec. Conf*, 2000.

[88] “WCT and FMT product series.” [Online]. Available: https://www.sintoninstruments.com/products/. [Accessed: 01-Feb-2022].

[89] M. J. Kerr, A. Cuevas, and R. A. Sinton, “Generalized analysis of quasi-steady-state and transient decay open circuit voltage measurements,” *J. Appl. Phys.*, vol. 91, no. 1, pp. 399–404, 2002.

[90] R. Sinton, D. De Ceuster, K. Wilson, and L. Rodrigues Barbosa, “Flash testing high-efficiency silicon solar cells and modules,” *20th Eur. Photovolt. Sol. Energy Conf.*, 2005.

[91] T. Roth *et al.*, “Illumination-induced errors associated with suns-VOC measurements of silicon solar cells,” *Rev. Sci. Instrum.*, vol. 80, no. 3, p. 33106, 2009.

[92] A. Cuevas and F. Recart, “Capacitive effects in quasi-steady-state voltage and lifetime measurements of silicon devices,” *J. Appl. Phys.*, vol. 98, no. 7, p. 74507, 2005.

[93] S. Glunz, J. Nekarda, H. Mäckel, and A. Cuevas, *Analyzing back contacts of silicon solar cells by Suns-Voc-measurements at high illumination densities*. 2007.

[94] O. Gunawan, T. Gokmen, and D. B. Mitzi, “Suns-VOC characteristics of high performance kesterite solar cells,” *J. Appl. Phys.*, vol. 116, no. 8, p. 84504, 2014.

[95] M. K. Forsyth, M. Mahaffey, A. L. Blum, W. A. Dobson, and R. A. Sinton, “Use of the Suns-Voc for diagnosing outdoor arrays amp; modules,” in *2014 IEEE 40th Photovoltaic Specialist Conference (PVSC)*, 2014, pp. 1928–1931.

[96] S. Guo, E. Schneller, J. Walters, K. O. Davis, and W. V Schoenfeld, “Detecting loss mechanisms of c-Si PV modules in-situ I-V measurement,” in *Reliability of Photovoltaic Cells, Modules, Components, and Systems IX*, 2016, vol. 9938, p. 99380N.

[97] A. Killam and S. Bowden, “Characterization of Modules and Arrays with Suns Voc,” in *2017 IEEE 44th Photovoltaic Specialist Conference (PVSC)*, 2017, pp. 2719–2722.

[98] J. Walters, S. Guo, E. Schneller, H. Seigneur, and M. Boyd, “PV module loss analysis using system in-situ monitoring data,” in *2018 IEEE 7th World Conference on Photovoltaic Energy Conversion (WCPEC) (A Joint Conference of 45th IEEE PVSC, 28th PVSEC 34th EU PVSEC)*, 2018, pp. 2204–2208.

[99] S. Nann and C. Riordan, “Solar spectral irradiance under overcast skies (solar cell performance effects),” in *IEEE Conference on Photovoltaic Specialists*, 1990, pp. 1110–1115 vol.2.

[100] T. Nordmann and L. Clavadetscher, “Understanding temperature effects on PV system performance,” in *3rd World Conference onPhotovoltaic Energy Conversion, 2003. Proceedings of*, 2003, vol. 3, pp. 2243-2246 Vol.3.

[101] D. Dirnberger, G. Blackburn, B. Müller, and C. Reise, “On the impact of solar spectral irradiance on the yield of different PV technologies,” *Sol. Energy Mater. Sol. Cells*, vol. 132, pp. 431–442, 2015.

[102] R. W. Andrews and J. M. Pearce, “The effect of spectral albedo on amorphous silicon and crystalline silicon solar photovoltaic device performance,” *Sol. Energy*, vol. 91, pp. 233–241, 2013.

[103] M. Mani and R. Pillai, “Impact of dust on solar photovoltaic (PV) performance: Research status, challenges and recommendations,” *Renew. Sustain. Energy Rev.*, vol. 14, no. 9, pp. 3124–3131, 2010.

[104] A. C. Killam, J. F. Karas, A. Augusto, and S. G. Bowden, “Monitoring of Photovoltaic System Performance Using Outdoor Suns-VOC,” *Joule*, vol. 5, no. 1, pp. 210–227, 2021.

[105] N. Blair *et al.*, “System Advisor Model (SAM) General Description (Version 2017.9.5),” Golden, CO, 2018.

[106] R. M. Smith, D. C. Jordan, and S. R. Kurtz, “Outdoor PV Module Degradation of Current-Voltage Parameters,” *Proc. 2012 World Renew. Energy Forum, Denver, Color.*, pp. 1–7, 2012.

[107] L. Dunn, M. Gostein, and K. Emery, “Comparison of pyranometers vs. PV reference cells for evaluation of PV array performance,” in *2012 38th IEEE Photovoltaic Specialists Conference*, 2012, pp. 2899–2904.

[108] M. Aminul Islam, N. M. Kassim, A. Ahmed Alkahtani, and N. Amin, *Assessing the Impact of Spectral Irradiance on the Performance of Different Photovoltaic Technologies*. IntechOpen, 2021.

[109] J. Zhou, Q. Yi, Y. Wang, and Z. Ye, “Temperature distribution of photovoltaic module based on finite element simulation,” *Sol. Energy*, vol. 111, pp. 97–103, 2015.

[110] Z. H. Lu, Q. Song, S. Q. Li, Q. Yao, and A. Othman, “The Effect of Non-Uniform Illumination on the Performance of Conventional Polycrystalline Silicon Solar Cell,” in *Proceedings of ISES World Congress 2007 (Vol. I -- Vol. V)*, 2009, pp. 1445–1448.

[111] W. Bludau, A. Onton, and W. Heinke, “Temperature dependence of the band gap of silicon,” *J. Appl. Phys.*, vol. 45, no. 4, pp. 1846–1848, 1974.

[112] M. Wang *et al.*, “Evaluation of Photovoltaic Module Performance Using Novel Data-driven I-V Feature Extraction and Suns-VOC Determined from Outdoor Time-Series I-V Curves,” 2018, pp. 778–783.

[113] F. T. Liu, K. M. Ting, and Z.-H. Zhou, “Isolation-Based Anomaly Detection,” *ACM Trans. Knowl. Discov. Data*, vol. 6, no. 1, Mar. 2012.

[114] K. McIntosh and C. Honsberg, “The Influence of Edge Recombination on a Solar Cell’s Iv Curve,” 2000.

[115] M. ~A. Green, “Solar cell fill factors: General graph and empirical expressions,” *Solid State Electron.*, vol. 24, no. 8, pp. 788–789, Aug. 1981.

[116] M. Leilaeioun and Z. C. Holman, “Accuracy of expressions for the fill factor of a solar cell in terms of open-circuit voltage and ideality factor,” *J. Appl. Phys.*, vol. 120, no. 12, p. 123111, 2016.

[117] X. Ma *et al.*, “Data-Driven I–V Feature Extraction for Photovoltaic Modules,” *IEEE J. Photovoltaics*, vol. 9, no. 5, pp. 1405–1412, 2019.

[118] S. Guo, F.-J. Ma, B. Hoex, A. G. Aberle, and M. Peters, “Analysing Solar Cells by Circuit Modelling,” *Energy Procedia*, vol. 25, pp. 28–33, 2012.

[119] D. B. Vandana Khanna Bijoy Kishore Das, “MATLAB/SIMELECTRONICS Models Based Study of Solar Cells,” *Int. J. Renew. Energy Res.*, vol. 3, pp. 30–34, 2013.

[120] S. R. Kurtz *et al.*, “Outdoor rating conditions for photovoltaic modules and systems,” *Sol. Energy Mater. Sol. Cells*, vol. 62, no. 4, pp. 379–391, 2000.

[121] G. Pfister, R. L. McKenzie, J. B. Liley, A. Thomas, B. W. Forgan, and C. N. Long, “Cloud Coverage Based on All-Sky Imaging and Its Impact on Surface Solar Irradiance,” 2003.

[122] D. Feldman, V. Ramasamy, R. Fu, A. Ramdas, J. Desai, and R. Margolis, “U.S. Solar Photovoltaic System and Energy Storage Cost Benchmark: Q1 2020,” Golden, CO, 2020.

[123] P. G. Loutzenhiser, H. Manz, C. Felsmann, P. A. Strachan, T. Frank, and G. M. Maxwell, “Empirical validation of models to compute solar irradiance on inclined surfaces for building energy simulation,” *Sol. Energy*, vol. 81, no. 2, pp. 254–267, 2007.

[124] A. Killam and S. Bowden, “Introducing Suns-VR as an enhancement to Suns-VOC for Characterizing Photovoltaic Cells and Modules,” in *2020 47th IEEE Photovoltaic Specialists Conference (PVSC)*, 2020, pp. 2181–2184.

[125] A. A. Willoughby, T. V Omotosho, and A. P. Aizebeokhai, “A simple resistive load I-V curve tracer for monitoring photovoltaic module characteristics,” in *2014 5th International Renewable Energy Congress (IREC)*, 2014, pp. 1–6.

[126] M. J. Morgan, G. Jakovidis, and I. McLeod, “An experiment to measure {theI}-Vcharacteristics of a silicon solar cell,” *Phys. Educ.*, vol. 29, no. 4, pp. 252–254, Jul. 1994.

[127] N. Martin and J. M. Ruiz, “Calculation of the PV modules angular losses under field conditions by means of an analytical model,” *Sol. Energy Mater. Sol. Cells*, vol. 70, no. 1, pp. 25–38, 2001.

[128] A. G. Siraki and P. Pillay, “Study of optimum tilt angles for solar panels in different latitudes for urban applications,” *Sol. Energy*, vol. 86, no. 6, pp. 1920–1928, 2012.

[129] R. A. Sinton and R. M. Swanson, “Recombination in highly injected silicon,” *IEEE Trans. Electron Devices*, vol. 34, no. 6, pp. 1380–1389, Jun. 1987.

[130] N. Keskitalo, P. Jonsson, K. Nordgren, H. Bleichner, and E. Nordlander, “Temperature and injection dependence of the Shockley–Read–Hall lifetime in electron-irradiated p-type silicon,” *J. Appl. Phys.*, vol. 83, no. 8, pp. 4206–4212, 1998.

[131] C. Buerhop *et al.*, “Evolution of cell cracks in PV-modules under field and laboratory conditions,” *Prog. Photovoltaics Res. Appl.*, vol. 26, no. 4, pp. 261–272, 2018.

[132] D. C. Jordan *et al.*, “Silicon Heterojunction System Field Performance,” *IEEE J. Photovoltaics*, vol. 8, no. 1, pp. 177–182, Jan. 2018.

[133] J. Coello, L. Perez, F. Domínguez, and M. Navarrete, “On-site Quality Control of Photovoltaic Modules with the PV MOBILE LAB,” *Energy Procedia*, vol. 57, 2014.

[134] K. Yedidi, S. Tatapudi, J. Mallineni, B. Knisely, J. Kutiche, and G. TamizhMani, “Failure and degradation modes and rates of PV modules in a hot-dry climate: Results after 16 years of field exposure,” in *2014 IEEE 40th Photovoltaic Specialist Conference (PVSC)*, 2014, pp. 3245–3247.

[135] G. TamizhMani, “Correlation of Qualification and Accelerated Testing with Field Degradation,” Mesa, 2018.

[136] G. TamizhMani, H. Field, M. Moorthy, A. Patankar, and S. Murali, “Simultaneous Non-contact I-V (NCIV) Measurements of Photovoltaic Substrings and Modules in a String,” in *2021 IEEE 48th Photovoltaic Specialists Conference (PVSC)*, 2021, pp. 1792–1794.

[137] J. E. Quiroz, J. S. Stein, C. K. Carmignani, and K. Gillispie, “In-situ module-level I–V tracers for novel PV monitoring,” in *2015 IEEE 42nd Photovoltaic Specialist Conference (PVSC)*, 2015, pp. 1–6.

[138] M. H. Ali, A. Rabhi, A. El Hajjaji, and G. M. Tina, “Real Time Fault Detection in Photovoltaic Systems,” *Energy Procedia*, vol. 111, pp. 914–923, 2017.

[139] C. B. Jones *et al.*, “Automatic fault classification of photovoltaic strings based on an in situ IV characterization system and a Gaussian process algorithm,” in *2016 IEEE 43rd Photovoltaic Specialists Conference (PVSC)*, 2016, pp. 1708–1713.

[140] P. Papageorgas, D. Piromalis, K. Antonakoglou, G. Vokas, D. Tseles, and K. G. Arvanitis, “Smart Solar Panels: In-situ Monitoring of Photovoltaic Panels based on Wired and Wireless Sensor Networks,” *Energy Procedia*, vol. 36, pp. 535–545, 2013.

[141] C. B. Jones, B. H. Ellis, J. S. Stein, and J. Walters, “Comparative Review of High Resolution Monitoring Versus Standard Inverter Data Acquisition for a Single Photovoltaic Power Plant,” in *2018 IEEE 7th World Conference on Photovoltaic Energy Conversion (WCPEC) (A Joint Conference of 45th IEEE PVSC, 28th PVSEC 34th EU PVSEC)*, 2018, pp. 715–720.

[142] M. Wang *et al.*, “Analytic Isc-Voc Method and Power Loss Modes From Outdoor Time-Series I-V Curves,” *IEEE J. Photovoltaics*, vol. PP, pp. 1–10, 2020.

[143] J. Liu *et al.*, “Real-world PV Module Degradation across Climate Zones Determined from Suns-Voc, Loss Factors and I-V Steps Analysis of Eight Years of I-V, Pmp Time-series Datastreams,” in *2019 IEEE 46th Photovoltaic Specialists Conference (PVSC)*, 2019, pp. 680–686.

[144] M. G. Deceglie, T. J. Silverman, B. Marion, and S. R. Kurtz, “Real-Time Series Resistance Monitoring in PV Systems Without the Need for I-V Curves,” *IEEE J. Photovoltaics*, vol. 5, no. 6, pp. 1706–1709, Nov. 2015.

[145] D. C. Jordan and S. R. Kurtz, “Photovoltaic degradation risk,” in *World Renewable Energy Forum, WREF 2012, Including World Renewable Energy Congress XII and Colorado Renewable Energy Society (CRES) Annual Conferen*, 2012, vol. 2, pp. 865–871.

[146] H. Haeberlin, “Normalized Representation of Energy and Power for Analysis of Performance and On-line Error Detection in PV-Systems,” 2003.

[147] A. Kimber *et al.*, “Improved test method to verify the power rating of a photovoltaic (PV) project,” in *2009 34th IEEE Photovoltaic Specialists Conference (PVSC)*, 2009, pp. 316–321.

[148] A. Phinikarides, N. Kindyni, G. Makrides, and G. E. Georghiou, “Review of photovoltaic degradation rate methodologies,” *Renew. Sustain. Energy Rev.*, vol. 40, pp. 143–152, 2014.

[149] X. Sun, R. V. K. Chavali, and M. A. Alam, “In-Situ Self-Monitoring of Real-Time

Photovoltaic Degradation Only Using Maximum Power Point: the Suns-Vmp Method," *arXiv Appl. Phys.*, 2018.

[150] S. Bowden *et al.*, "Agrivoltaics Citizen Science: A Model for Collaboration between Engineers and K-12 Schools," in *2021 IEEE 48th Photovoltaic Specialists Conference (PVSC)*, 2021, pp. 2146–2148.

[151] R. Hendarti, W. Wangidjaja, and L. G. Septiafani, "A study of solar energy for an aquaculture in Jakarta," *{IOP} Conf. Ser. Earth Environ. Sci.*, vol. 195, p. 12096, Dec. 2018.

[152] A. H. Alami *et al.*, "Novel and practical photovoltaic applications," *Therm. Sci. Eng. Prog.*, vol. 29, p. 101208, 2022.

[153] A. K. Shukla, K. Sudhakar, and P. Baredar, "Recent advancement in BIPV product technologies: A review," *Energy Build.*, vol. 140, pp. 188–195, 2017.

[154] R. Cazzaniga and M. Rosa-Clot, "The booming of floating PV," *Sol. Energy*, vol. 219, pp. 3–10, 2021.